



## Full Length Article

# Lab-scale pilot for CO<sub>2</sub> capture vacuum pressure swing adsorption: MIL-160(Al) vs zeolite 13X



A. Henrotin<sup>a</sup>, N. Heymans<sup>a</sup>, M.E. Duprez<sup>a</sup>, G. Mouchaham<sup>b</sup>, C. Serre<sup>b</sup>, D. Wong<sup>c</sup>, R. Robinson<sup>c</sup>, D. Mulrooney<sup>c</sup>, J. Casaban<sup>c</sup>, G. De Weireld<sup>a,\*</sup>

<sup>a</sup> Thermodynamics and Mathematical Physics Unit, University of Mons (UMONS), Place du parc 20, Mons 7000, Belgium

<sup>b</sup> Institut des Matériaux Poreux de Paris, École Normale Supérieure, ESPCI Paris, CNRS, PSL University, Paris 75005, France

<sup>c</sup> MOF Technologies Ltd, 63 University Road, Belfast BT7 1NF, United Kingdom

## ARTICLE INFO

## Keywords:

CO<sub>2</sub> capture  
Vacuum pressure swing adsorption  
Metal organic framework  
Zeolite  
Laboratory pilot

## ABSTRACT

Carbon capture is among the key technologies to quickly reduce anthropogenic CO<sub>2</sub> emissions to a net zero emission by 2050. Among the different separation technologies, adsorption is one of the most promising. Several Vacuum and/or Pressure Swing Adsorption cycles have been developed and tested for CO<sub>2</sub> capture using mainly zeolite 13X. Metal organic frameworks, due to their exceptional tunability, can improve the performance of adsorption processes. Nevertheless, there is a lack of experimental results for these materials at pilot scale. To address this gap, a versatile VPSA lab-scale pilot (3 columns of 1.1 L) has been developed to evaluate adsorbents at kilogram scale for CO<sub>2</sub> capture in various adsorption process configurations. The metal organic framework MIL 160(Al), synthesized and shaped at 60 kg, was also studied on this installation and compared to zeolite 13X with a 3-bed 6-step VPSA cycle for the separation of a 15/85 %vol of CO<sub>2</sub>/N<sub>2</sub> mixture between 0.1 and 2 bar. Results obtained reveal purity of 90 % and recovery of 92.7 % for the MIL-160(Al) while zeolite 13X only reaches 79.7 % of purity and 85 % of recovery, proving the efficiency of this material for CO<sub>2</sub> capture. These results contradict conventional indicators and demonstrate the importance of testing a material in VPSA cycle at kg scale to fully assess its performance.

## 1. Introduction

The greenhouse gas emissions, and particularly CO<sub>2</sub> anthropogenic emissions since industrial revolution are the main cause of climate change during the last decades. In order to reach the net zero emission in 2050 and limit the global warming to 1.5 °C, CO<sub>2</sub> emissions must be reduced to 20 GtCO<sub>2</sub>/yr in 2035 as stated by the Paris agreement, finalized during the COP26 in Glasgow, (IPCC, 2021; Rogelj et al., 2016; UNFCCC, 2022). In 2022, the global total anthropogenic CO<sub>2</sub> emissions were equal to 36.8 GtCO<sub>2</sub> with 90 % coming from fossil fuels, mainly for electricity and heat production (24.2 %) and industry sector (24.5 %) (IEA, 2023; Lamb et al., 2021).

In order to significantly reduce the CO<sub>2</sub> emissions during the transition between fossil fuels and renewable energy and for unavoidable CO<sub>2</sub> coming from industrial processes such as the carbonation of limestone in cement or lime processes, an efficient solution is the CO<sub>2</sub> capture preventing its release into the atmosphere. According to IEA projection, the carbon capture utilization and storage (CCUS) will capture 5.2 GtCO<sub>2</sub>/yr by 2050, with an important part of CO<sub>2</sub> reduction in several sectors such as cement production (63 %) and fuel transformation (86 %) (IEA,

2020). Post-combustion capture of CO<sub>2</sub> is the easiest, and currently the most popular configuration, due to the ability of retrofitting an existing plant. The targets generally used for performance indicators are 90 % of CO<sub>2</sub> recovery (recently 95 %) and 95 % of CO<sub>2</sub> purity as set from the U.S. department of energy (Hong, 2022; NETL, 2023). The CO<sub>2</sub> concentration of flue gases is ranging from 4 % for power plants using natural gas combined cycle to 15 % for coal fired plant. Higher CO<sub>2</sub> concentrations are found in cement kiln (17–33 %), lime kiln (20 %), and blast furnace (20–27 %) (Mondal et al., 2012; Sifat and Haseli, 2019; Simoni et al., 2022).

The most mature technology for CO<sub>2</sub> capture in post-combustion is the chemical absorption of CO<sub>2</sub> in amine-based solvent which is already deployed at commercial scale (*i.e.* Petra Nova and Boundary Dam). Aqueous solution containing 30 % of monoethanolamine (MEA) is the actual reference amine-based solvent; other solvents presenting interesting CO<sub>2</sub> capacity, kinetic, and heat of absorption are studied such as methyldiethanolamine (MDEA) or blend of MEA and piperazine. Research is still ongoing at smaller scale to find new solvents, and new less energy intensive capture process configurations. To our knowledge, the best energy consumption reported so far for this technology with MEA

\* Corresponding author.

E-mail address: [guy.deweireld@umons.ac.be](mailto:guy.deweireld@umons.ac.be) (G. De Weireld).

<https://doi.org/10.1016/j.ccst.2024.100224>

Received 13 February 2024; Received in revised form 30 April 2024; Accepted 1 May 2024

2772-6568/© 2024 The Author(s). Published by Elsevier Ltd on behalf of Institution of Chemical Engineers (IChemE). This is an open access article under the CC BY-NC-ND license (<http://creativecommons.org/licenses/by-nc-nd/4.0/>)

is 2.2 GJ/tCO<sub>2</sub> (Ahn et al., 2013; Hong, 2022; NETL, 2023; Vega et al., 2020). Nevertheless, the main drawbacks of this process is the toxicity and/or the dangerousness together with the degradation and the consumption of the solvent, in addition to the sensitivity to contaminants such as SO<sub>x</sub>, NO<sub>x</sub>, and oxygen (Bhattacharyya and Miller, 2017; Vega et al., 2020).

Other CO<sub>2</sub> capture technologies are being studied to overcome the disadvantage of absorption in amine solvent such as membranes, cryogenic processes, calcium looping, or clathrate hydrate but are still in an earlier stage of development compared to absorption (Hong, 2022; Kárászová et al., 2020; Sifat and Haseli, 2019; Song et al., 2019). CO<sub>2</sub> capture by adsorption consists in separating the CO<sub>2</sub> from the flue gas using the interactions between the surface of a porous solid and the gas. Adsorption using activated carbons or zeolites is already used in industrial applications such as hydrogen purification, air separation or petrochemical. Adsorption has been shown to be a serious competitor to capture in amine solvents due to the potentially lower energy required, cost, and environmental impact (Glier and Rubina, 2013; Khoo and Tan, 2006; Ruthven, 1984; Sifat and Haseli, 2019).

Commonly, in gas adsorption processes, the adsorbent is used in cyclic operation with an adsorption step followed by a regeneration of the adsorbent to remove the adsorbed compound. This can be achieved commonly by increase of temperature (Temperature Swing Adsorption (TSA)) or decrease of pressure (Pressure Swing Adsorption (PSA) or Vacuum Pressure Swing Adsorption (VPSA) if the regeneration is below atmospheric pressure) (Ruthven, 1984). The choice of the regeneration method depends on economic and technical considerations. (V)PSA processes are more suitable for rapid cycling operation and therefore the investment costs are limited. The main drawback of (V)PSA processes is the mechanical energy required to swing the pressure which is more expensive than the thermal energy but it could be provided by renewable electricity. Purity of the stream recovered during the regeneration step is also a concern in (V)PSA processes where the desorbed gas is mixed with the purge gas reducing the purity. As a rule of thumb, (V)PSA processes are preferred when the most adsorbed compound has a concentration higher than a few per cent in the feed gas which is the case for CO<sub>2</sub> capture (Grande, 2012; Ruthven, 1984; Sifat and Haseli, 2019).

Performance of adsorption processes are directly related to the material used. For post-combustion processes, zeolites such as 13X, NaY, 5A, NaZSM-5 that have high CO<sub>2</sub> adsorption capacities, selectivities and kinetics at low partial pressures of CO<sub>2</sub> (0.1–1 atm) and ambient temperature, look suitable for VPSA process. Nevertheless, these latter are sensitive to water due to their hydrophilic nature and contaminants such as SO<sub>x</sub> and NO<sub>x</sub>, reducing their capacity and active surface area. Activated carbons can also be used for carbon dioxide separation due to their high pore volumes and surface areas, in addition to their commercial availability and low costs. Nevertheless, their adsorption capacity is, in general, limited at low partial pressures of CO<sub>2</sub>, requiring working at higher pressure levels, thus, more suitable for PSA processes rather than VPSA. Also activated carbons are characterized by a low heat of adsorption, promoting an easy energy-effective sorbent regeneration of the material and, therefore, helping to preserve the sorbent integrity over adsorption cycles. They are also much less sensitive to water compared to zeolites due to their hydrophobic nature but the presence of contaminants such as SO<sub>x</sub> or NO<sub>x</sub> leads to a decrease of their performance. In addition, their CO<sub>2</sub>/N<sub>2</sub> selectivity (between 20 and 30) is slightly lower than zeolite 13X's one, although it can be increased by functionalizing their pores (Chue et al., 1995; Raganati et al., 2021; Riboldi and Bolland, 2017; Sumida et al., 2012). Metal organic frameworks (MOFs) are an emerging class of crystalline porous solids that have shown high promises as candidates for post-combustion CO<sub>2</sub> capture due to their highly modular structures allowing optimal features in terms of chemical compositions and pores geometry and dimensions as well as proven industrial scalability (Sumida et al., 2012; Younas et al., 2020). Among the MOFs studied for CO<sub>2</sub> capture, Mg-MOF-74, UTSA-16 and CALF-

20 can be, for instance, highlighted for their high CO<sub>2</sub> capacity at low partial pressures of CO<sub>2</sub> (>2 mmol/g at 0.15 bar) and their high selectivity (>100) (Hu et al., 2019; Lin et al., 2021; Younas et al., 2020). The stability of MOFs in the presence of water and contaminants is highly material-dependent. While Mg-MOF-74 and UTSA-16 exhibit a drastic decrease of CO<sub>2</sub> capacity in wet conditions, CALF-20 is almost insensitive to a water content (up to 20–30 % RH) (Yu and Balbuena, 2013; Lin et al., 2021; Masala et al., 2017).

Numerous (V)PSA processes have been developed for the separation of two gaseous compounds and can be applied for CO<sub>2</sub> capture in post-combustion. For the VPSA process to operate continuously, the real plant is composed of several beds going through different stages of the cycle. The simplest configuration for a (V)PSA process is the Skarstrom cycle consisting of an adsorption step of CO<sub>2</sub> at high pressure followed by a regeneration step at lower pressure to retrieve the CO<sub>2</sub> and a purge step with nitrogen to increase the recovery. An additional pressure equalization step can be used for increasing the efficiency of the process and reducing the energy consumption (Grande, 2012; Skarstrom, 1960). This cycle has been tested for CO<sub>2</sub> capture by simulation and/or experimentally with various adsorbents, including MOFs. Shen et al. (2011) tested this cycle without pressure equalization on an experimental VPSA pilot with 180 g of activated carbon with a mixture of 15/85 CO<sub>2</sub>/N<sub>2</sub> achieving a recovery ranging from 41.76 to 96.16 % and a purity of 43.6 to 63.0 %. To reach higher purity, the same pilot was used with 50 % of CO<sub>2</sub> at the inlet to represent a second unit of 2-stage capture unit, allowing to reach 90.1 to 93.7 % of purity but with a lower recovery (57.8–78.2 %). Zhao et al. (2017) performed the same cycle on a laboratory VPSA pilot containing 100 g of zeolite 13X with a CO<sub>2</sub>/N<sub>2</sub> mixture of 10 to 20 % of CO<sub>2</sub> reaching recovery between 57.4 and 90.4 % but without any information on purity. The same cycle was tested at laboratory scale (69.3 g) with the microporous Al terephthalate MOF MIL-53(Al) to compare the performance of this MOF to zeolite 13X and activated carbon. Results obtained for Al-MOF were better than activated carbon's but slightly lower than zeolite 13X's showing the CO<sub>2</sub> capture potential of MIL-53(Al) (Majchrzak-Kuceba et al., 2019). Alternatives to the Skarstrom cycle using different two-bed configurations have been tested in the literature to improve the performance of the capture process. A 2-bed 4-step cycle consisting of adsorption, co-current evacuation, counter-current evacuation, and pressurization has been widely studied for CO<sub>2</sub> capture in post-combustion. The co-current evacuation aims to remove the nitrogen from the adsorption column by decreasing the pressure to a higher value than the counter-current evacuation (Grande, 2012; Haghpanah et al., 2013a). This cycle can be improved by modifying or adding new steps such as pressure equalization, purge (light product reflux) or rinse with CO<sub>2</sub> (heavy product reflux). Haghpanah et al. (2013b) have studied different configurations of this cycle for zeolite 13X, and have identified the 4-step cycle with light product pressurization as the most efficient one in terms of recovery, purity and energy consumption. This cycle was experimentally validated in a pilot containing 41 kg of zeolite 13X and treating a flue gas containing 15 % of CO<sub>2</sub> and 85 % of N<sub>2</sub> with a flow rate of 57 Nm<sup>3</sup>/h, reaching 86.4 % of recovery and 95.9 % of purity for an energy consumption of 472 kWh/tCO<sub>2</sub>. It should be noted that the vacuum pressure used for this optimum is 0.011 bar. Moreover, the flue gas is not treated during the whole cycle due to a regeneration time longer than the adsorption time (Krishnamurthy et al., 2014). Different adsorbents have been tested with this cycle by simulation. Mg-MOF-74 and UTSA-16 provide similar performance compared to zeolite 13X on this cycle, confirming their potential (Rajagopalan et al., 2016). CALF-20 has also been tested with this cycle with a laboratory pilot containing 36 g of adsorbent, reaching a recovery of 90 % with a purity of 85 % for a moderate energy consumption of 176 kWh/tCO<sub>2</sub>. Nevertheless, the cycle used does not allow a continuous treatment of the flue gas, in addition to a low level of vacuum needed (0.03 bar) to reach these results (Nguyen et al., 2022, 2023). A major disadvantage of this cycle is that it has mainly been tested at relatively low desorption pressures (optima

are around 0.03 bar). Yu et al. (2022) have recently tested a similar cycle with a pressure equalization step on a two-stage VPSA pilot with an evacuation pressure of 0.1 bar. The first stage used 1.49 kg of carbon molecular sieve, and the second one 0.44 kg of zeolite 13X. The overall process was able to reach a recovery of 88.3 to 94.6 % and a purity of 92.3 to 96.0 % for an energy consumption of 280 to 368 kWh/t<sub>CO<sub>2</sub></sub>. Khurana & Farooq (2016) have proposed a 6-step cycle with dual reflux and tested it with zeolite 13X and UTSA-16. The cycle was able to reach 95 % of purity and 90 % of recovery for both adsorbents with an evacuation pressure of 0.2 bar which is more suitable for industrial processes. Nevertheless, the light reflux step leads to an increase of the energy consumption compared to the 4-step cycle, giving an increase of 36 % from the 0.02 bar case (4-step) to the 0.2 bar case (6-step) for a recovery of 90 % and a purity of 95 %.

Complex cycle with only two adsorption beds can be difficult to synchronize, leading to idle of the adsorption column and a decrease of the productivity of the unit. To overcome this issue, more adsorption beds can be used to have a continuous treatment of the flue gas. The same steps as the 2-bed cycle (pressurization, adsorption, evacuation, reflux, ...) can be used in a 3-bed or 4-bed configuration (Grande, 2012). Several cycle configurations have been tested with three adsorption beds. Zhang et al. (2008) studied a 3-bed 6-step configuration including two pressure equalization steps and a 3-bed 9-step configuration adding a heavy product reflux and a light product pressurization. The laboratory pilot was filled with 3.61 kg of zeolite 13X treating a flue gas containing 12 % of CO<sub>2</sub> and was able to reach a recovery of 60 to 80 % and purity of 82 to 83 % for the 6-step cycle, and a recovery of 60 to 70 % and purity of 90–95 % for the 9-step cycle. The latter is able to produce higher purity due to the reflux step, with an energy consumption increase (40 to 50 %) compared to the 6-step cycle. A 3-bed 5-step cycle with zeolite 13X containing adsorption, heavy reflux, counter-current evacuation, light reflux and pressurization steps was studied by simulation as a first unit by Wang et al. (2012). Results from the 3-bed unit were used as initial conditions of a two-bed pilot used to study a two stages VPSA. The first unit was able to obtain a recovery of 98.92 % for a purity of 65.38 %, allowing the whole capture unit to reach the target of 95 % of purity and 90 % of recovery. A 3-bed 8-step cycle was tested on coal-fired power plant with zeolite 5A (93.9 kg per column) (Liu et al., 2012), and zeolite 13X (87 kg per column) (Wang et al., 2013) with a flue gas containing 15 to 16.5 % of CO<sub>2</sub> and a flow rate of 32 to 47 Nm<sup>3</sup>/h. The 8-step cycle is composed of a pressurization, adsorption, co-current evacuation, heavy reflux, pressure equalization, counter-current evacuation, and light reflux steps. The unit was able to reach 79 to 91 % recovery with zeolite 5A, and 84 to 95 % with zeolite 13X for a similar purity (71–85 %). Four beds installation are not usually studied for post-combustion CO<sub>2</sub> capture. The only reported pilot with four beds uses a cycle with nine steps including two pressure equalization and heavy product reflux steps, and 195 g of zeolite 13X per bed. The installation was able to reach a recovery of 51.3 to 88.0 % for a flue gas of 15 % CO<sub>2</sub>, and a purity between 88.0 and 96.7 % (Webley et al., 2017). In addition to the pilot presented above, newly developed materials have been tested with single column experiments to evaluate the performance with a small amount of material. UiO-66 performances for CO<sub>2</sub> capture have been evaluated with 5-step cycle with pressurization, adsorption, heavy reflux, counter-current evacuation, and light reflux. The MOF was able to reach up to 54.2 % of purity and 54.1 % of recovery (Edubilli and Gumma, 2019). The same MOF was studied on a 6-step cycle with pressurization, adsorption, co-current evacuation, heavy reflux, counter-current evacuation, and light reflux. The results obtained are slightly better with a recovery of 60–70 % and purity of 60 %. Nevertheless, the evacuation pressure and mass of adsorbent are not clearly given (8.25 cm<sup>3</sup> of volume) which make the complete comparison difficult (Andersen et al., 2013). CuBTC was also studied on the same installation giving recoveries between 62 and 64 % and purities of 60–70 % which are better than those related to UiO-66 (Dasgupta et al., 2012). VPSA cycle found in literature and discussed above are listed in

Table 1, giving the operating conditions and the results obtained when available.

In this work, a home-made versatile laboratory-scale VPSA pilot was developed to evaluate the performance of commercial or innovative adsorbents at kilogram scale for the CO<sub>2</sub>/N<sub>2</sub> separation with different cycle configurations. The pilot developed is able to work with two or three adsorption columns and can perform the different steps of an adsorption cycle: adsorption, counter and co-current evacuation, light and heavy reflux, feed or light product pressurization, and pressure equalization. The 6-step cycle developed by Khurana & Farooq (2016) was chosen due to its ability to provide high recoveries and purities with a moderate level of vacuum (0.1 bar) which is more representative of the level of vacuum in industrial processes, and was adapted to work with three columns to treat the flue gas in continuous. This cycle was tested with the benchmark material zeolite 13X and one representative robust MOF. This latter has been selected in the framework of the European project MOF4AIR (Heymans et al., 2021) in which several benchmark MOFs, showing various features have been synthesized and tested at different scales to identify the most promising materials for CO<sub>2</sub> capture in realistic conditions. Among, these MOFs, MIL-160(Al) (Cadiou et al., 2015) was selected, studied at g-scale and 100 g-scale before being produced at 60 kg scale for industrial pilot testing, and 3 kg among the 60 kg were used for studies on the laboratory-scale VPSA pilot. The MIL-160(Al), of formula Al(OH)(O<sub>2</sub>C-C<sub>4</sub>H<sub>2</sub>O-CO<sub>2</sub>), is a microporous MOF built up from helical chains of corner-shared AlO<sub>6</sub> polyhedral linked together via the five-membered rings biderived FDCA or 2,5 furan di-carboxylate ligand, delimiting narrow 1D channel of pore size between 4 and 6 Å. It possesses BET surface of 1220 m<sup>2</sup>/g and a pore volume of 0.404 cm<sup>3</sup>/g, while polar-OH Bronsted sites decorate the inorganic chains allowing favorable (Van der Waals) interactions with CO<sub>2</sub> (or H<sub>2</sub>O) molecules which provide a high selectivity between N<sub>2</sub> and CO<sub>2</sub>. The adsorption enthalpy for CO<sub>2</sub> is equal to -33 kJ/mol, allowing easier regeneration. Adsorption capacity for CO<sub>2</sub> is equal to 0.95 mmol/g at 30 °C and 0.15 bar, giving a working capacity of 0.85 mmol/g between 0.015 and 0.15 bar. The IAST (Ideal Adsorption Solution Theory) selectivity of this MOF for a 15/85 CO<sub>2</sub>/N<sub>2</sub> mixture is equal to 34 for a pressure of 1 bar and a temperature of 303 K (Damasceno Borges et al., 2017). Moreover, MIL-160(Al) can be produced under green conditions (in water under atmospheric pressure), at the kg-scale (Permyakova et al., 2017). It is rather stable in water and under steam (Wahiduzzaman et al., 2018) and has also been reported to be resistant to SO<sub>2</sub> where adsorption occurs for this compound with a higher selectivity than CO<sub>2</sub> (Brandt et al., 2019; Lyu and Maurin, 2021). Karimi et al. (2023) have studied the MIL-160(Al) for CO<sub>2</sub>/N<sub>2</sub> separation, showing interesting properties such as the low heat of adsorption for CO<sub>2</sub>, the relatively fast mass transfer, and the working capacity, in addition to the scalability of the MOF, the cost and the stability for industrial application.

## 2. Material and methods

### 2.1. VPSA pilot

The VPSA pilot developed aims to test adsorbents, define more appropriate VPSA configurations, optimize the operating conditions (design of experiments), and reproduce the behavior of an industrial VPSA pilot at the scale of 0.5 to 1.5 Nm<sup>3</sup>/h of flue gas. The pilot comprises a gas generation system, three adsorption beds, a vacuum pump, and a compressor, allowing the operation in different configurations such as 2-bed 4-step, 3-bed 5-step, and 3-bed 6-step. The VPSA pilot is also fully instrumented, providing measurements of temperature, pressure, gas composition, and flow rate at various key points. The whole flow-sheet of the VPSA pilot is represented in Fig. 1.

The CO<sub>2</sub>/N<sub>2</sub> gas mixture is generated by two thermal mass flow controllers (Bronkorst F-201AV) with a full scale of 3 Nm<sup>3</sup>/h for nitrogen and 1 Nm<sup>3</sup>/h for CO<sub>2</sub>. CO<sub>2</sub> and N<sub>2</sub> come from gas cylinders with a purity higher than 99.999 % (Air Liquide). A flow meter (Brooks SLA5860

**Table 1**  
 Experimental and simulation of VPSA cycles in literature. 4-step<sup>(1)</sup> : adsorption, evacuation, light reflux, pressurization ; 4-step<sup>(2)</sup> : adsorption, co-current evacuation, counter-current evacuation, light product pressurization ; 4-step<sup>(3)</sup> : adsorption, equalization, evacuation, pressurization ; 6-step<sup>(1)</sup> : adsorption, heavy reflux, co-current evacuation, counter-current evacuation, light reflux, pressurization ; 6-step<sup>(2)</sup> : adsorption, equalization, heavy reflux, evacuation, pressurization 1, pressurization 2 ; 6-step<sup>(3)</sup> : pressurization, adsorption, co-current evacuation, heavy reflux, counter-current evacuation, and light reflux. The star exponent (\*) denotes simulation or experiment of a single bed without considering the synchronization of multiple beds. The P and S in type denote for pilot and simulation.

Cycle	Type	Adsorbent	Flow rate [Nm <sup>3</sup> /h]	CO <sub>2</sub> concentration [%]	Adsorption pressure [bar]	Evacuation pressure [bar]	Mass [kg]	Recovery [%]	Purity [%]	Productivity [tCO <sub>2</sub> /m <sup>3</sup> /day]	Energy kWh/tCO <sub>2</sub>	Refs.
2-bed 4-step <sup>(2)</sup>	P	Zeolite 13X	56.9	15	1.5	0.025–0.009	41	83.4–96.3	85.4–94.5	0.87–1.4	339–582	(Krishnamurthy et al., 2014)
4-step <sup>(2)*</sup>	S	AC	5.4–108.2	15	1	0.03	13.1	80–95	80–93	/	/	(Rajagopalan et al., 2016)
4-step <sup>(2)*</sup>	S	Zeolite 13X	5.4–108.2	15	1	0.03	18.5	80–99	80–98	1.37–3.50	135–156	(Rajagopalan et al., 2016)
4-step <sup>(2)*</sup>	S	Mg-MOF-74	5.4–108.2	15	1	0.03	9.6	80–98	80–97	1.01–1.68	177–242	(Rajagopalan et al., 2016)
4-step <sup>(2)*</sup>	S	UTSA-16	5.4–108.2	15	1	0.03	17.9	80–99	80–99	2.18–2.81	116–120	(Rajagopalan et al., 2016)
4-step <sup>(2)*</sup>	S	CALF-20	5.4–108.2	15	1	0.03	5.6	80–98	80–99	/	/	(Nguyen et al., 2022)
2-bed 4-step <sup>(2)</sup>	P	CALF-20	0.05–0.11	15	1	0.031	0.036	83.1–92.4	80.6–97.2	0.49–1.14	140–192	(Nguyen et al., 2023)
3-bed 8-step	P	Zeolite 5A	32–46	15	1.2	0.05	93.9	79–91	71–85	0.47–0.78	733–867	(Liu et al., 2012)
3-bed 8-step	P	Zeolite 13XAPG	33–47	15.5–16.5	1.17	0.07	87	84.7–95.2	71–85	0.52–0.84	497–867	(Wang et al., 2013)
2-bed 4-step <sup>(1)</sup>	P	AC	0.057–0.171	15	1.31–3.24	0.03–0.1	0.18	41.8–96.2	43.6–63.0	0.93–1.71	/	(Shen et al., 2011)
2-bed 4-step <sup>(1)</sup>	P	AC	0.057–0.171	50	1.31–3.24	0.03–0.1	0.18	57.8–78.2	90.1–93.7	3.29–3.94	/	(Shen et al., 2011)
2-bed 4-step <sup>(1)</sup>	P	MIL-53(Al)	0.01	16	1.25	0.1–0.2	0.069	10.0–80.0	39.5–60	/	/	(Majchrzak-Kuceba et al., 2019)
2-bed 4-step <sup>(3)</sup> (2 stages)	P	CMS + 13X	1.26–1.46	12 - 16	1.2–1.4	0.1	1.49 (stage 1) - 0.44 (stage 2)	88.3 - 94.6 (overall)	92.3 - 96.0	2.07–2.83	280–368	(X. Yu et al., 2022)
4-bed 6-step	P	Zeolite 13X	0.32	15	1.1	0.05–0.08	0.19	51.3–88.0	88.0–96.7	1.16 - 2.15	86–97	(Webley et al., 2017)
3-bed 5-step	S	Zeolite 13XAPG	0.051 - 0.190	15	1.5	0.06–0.15	0.13	39.0–99.9	59.2–77.4	0.35 - 0.60	98 - 159	(Wang et al., 2012)
2-bed 4-step <sup>(1)</sup>	P	Zeolite 13X	0.0569 - 0.171	10–20	1.8	/	0.1	57.4–90.4	/	/	755	(Zhao et al., 2017)
3-bed 4-step	P	Zeolite 13X	3.96–6.9	8–22	1.35	0.03–0.06	3.61	60–80	82–83	/	80–120	(Zhang et al., 2008)
3-bed 6-step <sup>(2)</sup>	P	Zeolite 13X	3.96–6.9	8–22	1.35	0.03–0.06	3.61	60–70	90–95	/	120–170	(Zhang et al., 2008)
6-step <sup>(1)*</sup>	S	Zeolite 13X	5.4–162.3	15	1	0.005–0.2	18.5	>90	>95	2.84–8.82	159–216	(Khurana and Farooq, 2016)
6-step <sup>(1)*</sup>	S	UTSA-16	5.4–162.3	15	1	0.005–0.2	17.9	>90	>95	7.94–18.06	131–176	(Khurana and Farooq, 2016)
5-step*	P	UiO-66	0.003–0.012	15	1.3	0.15	0.0093	54.1	54.2	/	/	(Edubilli and Gumma, 2019)
6-step <sup>(3)*</sup>	P	UiO-66	0.0156	15	2	/	/	60–70	60	/	/	(Andersen et al., 2013)
6-step <sup>(3)*</sup>	P	CuBTC	0.0156	13–16	2	0.15	/	62–64	60–70	/	/	(Dasgupta et al., 2012)

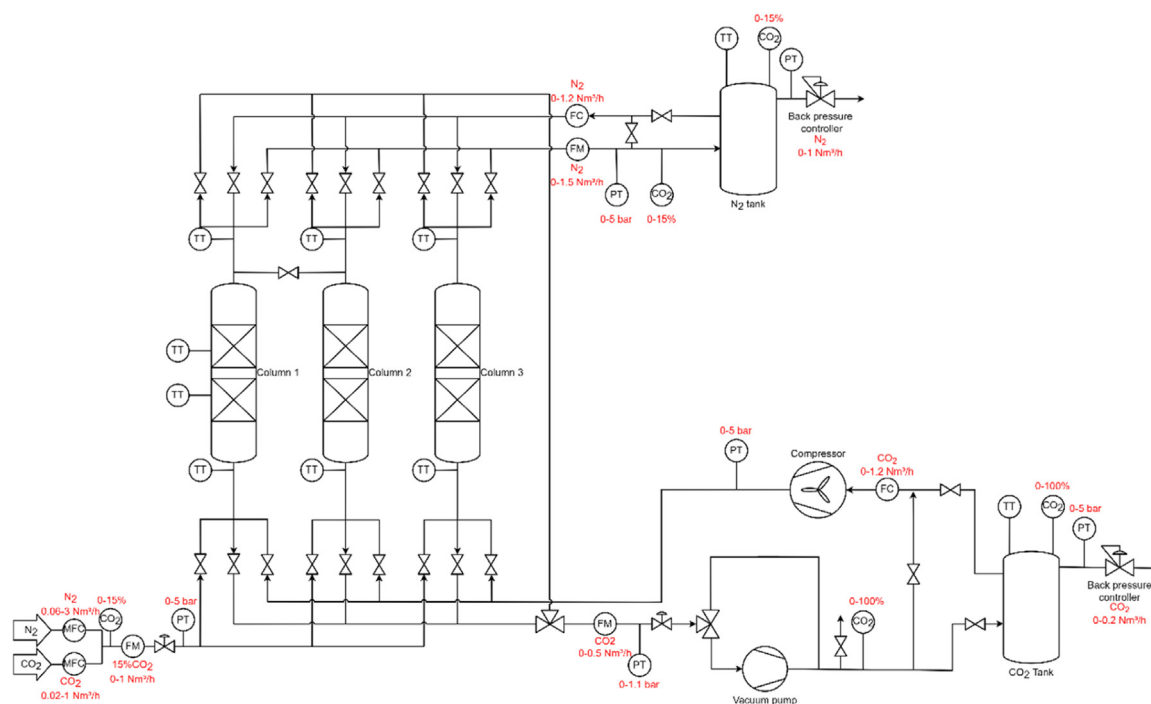


Fig. 1. Flowsheet of the VPSA pilot.

with a full-scale of  $1.5 \text{ Nm}^3/\text{h}$  and calibrated for 15 %  $\text{CO}_2$  / 85 %  $\text{N}_2$ ) allows the measurement of the gas mixture total flow rate and to check that the generated flow matches the setpoint. The  $\text{CO}_2$  concentration of the flow can also be measured after generation. Then, the gas flows through a proportional valve (Asco 202) which can be modulated for pressurization steps. Also, a pressure transmitter (Retec ATMECO with a range of 0–5 bar abs) is set to measure the pressure before the adsorption beds.

The generated gas is sent to the column section which contains a total of 19 valves (Asco 263) where six are used to direct the gas flow to the different sections of the installation and one supplementary for the equalization between two columns. The three adsorption columns have a length of 30 cm and a diameter of 7.01 cm giving a volume of 1.157 L and L/D ratio of 4.28. Filters at the ends of the columns retain the adsorbent in the column and evenly distribute the gas. Each adsorption bed is equipped with temperature sensors (type K thermocouple) at the inlet and the outlet of the bed. Column 1 is equipped with an immersion sleeve to measure the temperature inside the column (Type K thermocouple) at 5 cm and 25 cm starting from the bottom of the adsorption layer. Columns 2 and 3 can be isolated with manual valves to work with one (breakthrough curves) or two columns.

The flow coming from the top of the adsorption columns is measured with a flow meter (Brooks SLA5860 with a full-scale of  $1.5 \text{ Nm}^3/\text{h}$  and calibrated for 100 %  $\text{N}_2$ ), in addition with a measurement of pressure and  $\text{CO}_2$  concentration. After the flow meter, a valve can be opened to reuse a part of this flow for light reflux step. In this case, a flow controller (Brooks SLA5850 with a full-scale of  $1.2 \text{ Nm}^3/\text{h}$  and calibrated for 100 %  $\text{N}_2$ ) is used to regulate the flow of the reflux. The flow which is not used for the reflux is sent to a tank of 500 L to store the gas. The tank is equipped with a temperature sensor (Pt100), a pressure transmitter (Retec ATMECO with a range of 0–5 bar abs) and is connected to the gas analyzer. The tank has two outlets, the first one used for light reflux if this step is not synchronized with an adsorption step. The second one is connected to a back pressure controller (Brooks 5866RC with a full-scale of  $1 \text{ Nm}^3/\text{h}$  and calibrated for 100 %  $\text{N}_2$ ). This controller allows keeping a constant pressure in the nitrogen tank thus setting the adsorption pressure of the VPSA process.

Evacuation is performed by connecting the bottom or the top of the columns to the vacuum pump of the pilot using a 3-way valve (Asco 327). A flow meter (Brooks SLA5860 with a full-scale of  $0.5 \text{ Nm}^3/\text{h}$  and calibrated for 100 %  $\text{CO}_2$ ) is used, followed by a Pirani gauge for pressure measurement under vacuum (Pfeiffer Vacuum CMR 361 with a range of 0.1 to 1100 mbar), and a proportional valve (Asco 202). This valve is used to regulate the pressure during the blowdown steps based on the measurement of the Pirani gauge. A second 3-way valve (Asco 327) is used to bypass the vacuum pump when the pressure is higher than the  $\text{CO}_2$  tank pressure to prevent damage on the pump. The vacuum pump used is the HiScroll 6 from Pfeiffer Vacuum. This pump is dry and oil-free to avoid contaminants in the adsorption columns and has a pumping speed of  $6.1 \text{ m}^3/\text{h}$  at atmospheric pressure, and a typical lowest pressure of 2 Pa. The speed of the pump can be adjusted by numerical communication, allowing to reduce the speed during the co-current evacuation step to reach a set-up pressure value. To regulate and maintain a pressure setpoint during blowdown and purge steps, a PID controller is used to control the opening of the proportional valve according to the pressure measurement and setpoint. After the vacuum pump, the flow concentration can be analyzed and is sent to an atmospheric vent (co-current evacuation) or to the  $\text{CO}_2$  tank (counter-current evacuation) or used for heavy reflux by connecting the flow the mass flow controller (Brooks SLA5850 with a full-scale of  $1.2 \text{ Nm}^3/\text{h}$  and calibrated for 100 %  $\text{CO}_2$ ). The  $\text{CO}_2$  tank (200 L) configuration is like the nitrogen tank: temperature, pressure and concentration are analyzed inside the tank, and a back pressure controller (Brooks 5866RC with a full-scale of  $0.2 \text{ Nm}^3/\text{h}$  and calibrated for 100 %  $\text{CO}_2$ ) allows to keep a constant pressure in the  $\text{CO}_2$  tank. The  $\text{CO}_2$  store in the tank can be reused for heavy reflux if this step is not synchronized with evacuation or light reflux. For heavy reflux, the compressor used is a N922STE diaphragm pump from KNF. This pump allows to reach a maximum pressure of 5 bar (absolute), with a flow rate of  $9.5 \text{ L}/\text{min}$  at this pressure. At atmospheric pressure, the maximum flow rate is equal to  $21 \text{ L}/\text{min}$ . A pressure transmitter (Retec ATMECO with a range of 0–5 bar abs) allows to measure the pressure generated by the compressor.

The gases are analyzed by a four-channel NDIR analyzer (Emerson X-STREAM Enhanced) with a measuring range of 0–100 %  $\text{CO}_2$ . All the

channels were calibrated with a 99.999 % N<sub>2</sub> gas for zeroing. Channels one and two which were calibrated with a gas mixture containing 15 % CO<sub>2</sub> / 85 % N<sub>2</sub> with 2 % of relative uncertainties on concentrations for measurement of gas with less than 15 % of CO<sub>2</sub> concentration. The two other channels were calibrated with 99.999 % CO<sub>2</sub> gas. A correction based on the density of the analyzed gas must be applied on the value obtained from the analyzer. This correction is based on the pressure of the gas since the analyzer is maintained to 70 °C.

Five sampling points exist on the pilot (CO<sub>2</sub> in Fig. 1). Inlet and outlet of channel 1 are connected to the nitrogen tank, making a continuous analysis of the tank concentration. The circulation of the gas is assured by a pump (KNF NMP830 with a maximum flow rate of 3.1 L/min) with a variable motor speed. The inlet of channel 2 is connected to the gas generation, top of the column and outlet of the vacuum pump (used during co-current evacuation). The outlet of this channel can be connected to the atmosphere or the nitrogen tank. Channel 3 comes from the outlet of vacuum pump and is used during evacuation or reflux step. The channel 4 inlet is connected to the CO<sub>2</sub> tank. Both channel 3 and 4 outlets are connected to the CO<sub>2</sub> tank. As for channel 1, a circulation pump is used for channel 4.

The operating of the VPSA pilot is provided by a programmable logic controller (Wago PFC100), allowing to record temperature, pressure, flow rate, and gas concentration, to receive the different signals from the equipment, to record the data, and to control manually or automatically the installation (valves, flow controllers, vacuum pump, circulation pump, compressor, backpressure controllers). A homemade software was developed on "e-cockpit" (software provided by Wago) to allow communication between the elements of the pilot, and to provide a graphical user interface. The interface allows to control individually each component, but also to define the VPSA cycle to perform by giving the cycle parameters. The software developed allows to record temperature, pressure, flow, and concentration every second. During the operation of a cycle, purity and recovery are computed from the flow and concentration recorded to represent the evolution of both indicators for each completion of a cycle, allowing to determine when the pilot is in steady state.

## 2.2. VPSA cycle

The VPSA cycle used is adapted from the 6-step cycle of [Khurana & Farooq \(2016\)](#) to work with three adsorption beds in order to have a continuous treatment of the flue gas. The configuration of the cycle is represented in [Fig. 2](#) with a schematic representation of the pressure level for the first adsorption bed.

Several relationships exist between the duration of each step to synchronize the three beds. As represented in [Fig. 2](#), adsorption time ( $t_{adsorption}$ ) must be equal to the sum of light reflux ( $t_{LR}$ ) and light product pressurization ( $t_{LPP}$ ) times. Also, light product pressurization time must be equal to the co-current evacuation time ( $t_{co-current\ evacuation}$ ) and counter-current evacuation times ( $t_{counter-current\ evacuation}$ ). Finally, the light and heavy reflux steps must have the same duration as the flow coming from the column in light reflux step is used for the heavy reflux. Therefore, the cycle is completely defined with only three parameters: adsorption time, reflux time, and co-current evacuation time. Light product pressurization and counter-current evacuation times are given by [Eqs. \(1\) and \(2\)](#).

$$t_{LPP} = t_{adsorption} - t_{LR} \quad (1)$$

$$t_{counter-current\ evacuation} = t_{adsorption} - t_{LR} - t_{co-current\ evacuation} \quad (2)$$

In addition to the three times selected to define the VPSA cycle, adsorption pressure, co- and counter-current evacuation pressures, and reflux flow rate can be modified to study the impact of these parameters on the VPSA pilot. In the present work, cycle time, reflux flow rate and co-current evacuation pressure were studied to determine the impact of these parameters on the VPSA pilot. Adsorption pressure was

set to 2 bar based on preliminary works to obtain good separation performance for both adsorbents. Counter-current evacuation pressure was kept at 0.1 bar which is a realistic vacuum level for industrial applications.

Performances of VPSA pilot were usually evaluated by two indicators: recovery and purity. The recovery gives the percentage of CO<sub>2</sub> retrieved in the product stream compared to the amount of CO<sub>2</sub> in the feed gas. The purity is the mean purity of the CO<sub>2</sub> obtained at the outlet of the process.

For purity, the flow rate measured with the back pressure controller of the CO<sub>2</sub> tank ( $Q_{BPC\ CO_2}$ ), and the concentration of the gas in the tank ( $y_{CO_2\ tank}$ ) are used for the calculation. Purity is obtained by summing the product of the flow rate measured by the back pressure controller and the concentration of CO<sub>2</sub> tank. This sum is divided by the sum of the back pressure flow rate ([Eq. \(3\)](#)).

$$Purity = \frac{\sum_{cycle} Q_{BPC\ CO_2} \cdot y_{CO_2\ tank}}{\sum_{cycle} Q_{BPC\ CO_2}} \quad (3)$$

Recovery is obtained by summing the product of the flow rate measured by the back pressure controller and the concentration of CO<sub>2</sub> tank. This sum is divided by the sum of CO<sub>2</sub> flow rate measured by the CO<sub>2</sub> controller at the inlet of the VPSA pilot ( $Q_{feed\ CO_2}$ ).

$$Recovery = \frac{\sum_{cycle} Q_{BPC\ CO_2} \cdot y_{CO_2\ tank}}{\sum_{cycle} Q_{feed\ CO_2}} \quad (4)$$

Productivity, another key indicator, is calculated by taking the amount of CO<sub>2</sub> obtained during one cycle in the same way as the recovery calculation, divided by the volume of adsorbent ( $V_{ads}$ ) and the time of the cycle ( $t_{cycle}$ ). To compare the obtained value to those listed in [Table 1](#), the productivity is expressed in  $t_{CO_2}/(m^3 \cdot day)$ . [Eq. \(5\)](#) gives the expression of the productivity.

$$Productivity = \frac{\sum_{cycle} Q_{BPC\ CO_2} \cdot y_{CO_2\ tank}}{V_{ads} \cdot t_{cycle}} \quad (5)$$

Uncertainties were also calculated for the three indicators. The complete calculation is available in section 1 of Supporting Information. The cycle is stopped when the increase of purity and recovery is less than 0.1 % per cycle which is generally obtained after 30 to 40 cycles. In addition to purity, recovery and productivity, the energy consumption of the pilot was estimated.

The energy consumption of compression was estimated with the [Eq. \(6\)](#) for the compression of the feed flow rate, the vacuum pump, and the rinse compressor.

$$E = \frac{Q \cdot R \cdot T}{\eta} \frac{\gamma}{\gamma - 1} \left( \left( \frac{p_2}{p_1} \right)^{\frac{\gamma-1}{\gamma}} - 1 \right) \quad (6)$$

With  $E$  the energy consumption (J),  $Q$  the flow rate (mol/s),  $R$  the gas constant (8.314 J/(mol.K)),  $T$  the gas temperature before compression (K),  $\gamma$  the heat capacity ratio of the gas,  $p$  the pressure (bar) with subscript 1 before the compression and 2 after compression, and  $\eta$  the efficiency equal to 0.85 for compression and 0.75 for vacuum pump. The energies obtained are summed and divided by the amount of CO<sub>2</sub> captured. For comparison with [Table 1's](#) values, the energies are expressed in kWh/ $t_{CO_2}$ . Since the energy consumption calculation is theoretical, the uncertainties were not computed for this indicator.

The number of parameters to study and their values can lead to an infinity of possible experiments to completely study the VPSA cycle. Since VPSA experiments are time consuming, a design of experiments was performed to study purity and recovery on the VPSA pilot with a reasonable number of experiments for zeolite 13X and MIL-160(Al). Five variables were studied to study their impact on the pilot for the separation of a flue gas containing 15/85 %vol. of CO<sub>2</sub>/N<sub>2</sub> mixture with a flow rate of 1 Nm<sup>3</sup>/h: Adsorption time [100–230 s], light reflux time [40–150 s], co-current evacuation time [20–40 s], light reflux flow rate

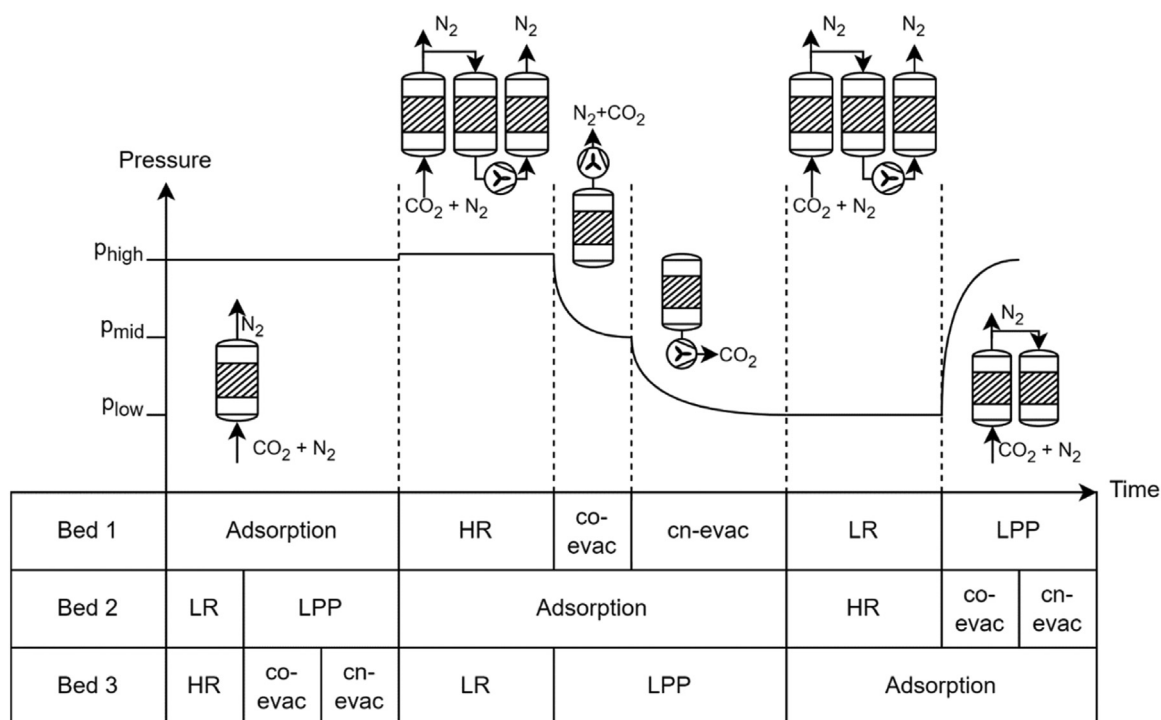


Fig. 2. Cycle configuration of the 3-bed 6-step cycle with pressure level representation of bed 1 (HR: heavy reflux, co-evac: co-current evacuation, cn-evac: counter-current evacuation, LR: light reflux, LPP: light product pressurization). The size of the blocks is not representative of the duration of the steps.

[0.1–0.3 Nm<sup>3</sup>/h] and co-current evacuation pressure [0.4–0.6 bar]. Adsorption time bounds were chosen, based on the breakthrough time of MIL-160(Al) which is 130 s for a pressure of 1.39 bar (see Section 3.1). The bounds of adsorption time were then increased since the VPSA cycle is performed for an adsorption pressure of 2 bar (breakthrough time of 170 s). Light reflux time was adapted from the adsorption time by taking lower values than bounds of adsorption time. 40 s was chosen to have a sufficient regeneration of the bed during the light reflux, and upper bound of 150 s to limit the amount of CO<sub>2</sub> sent in the column during the heavy reflux step. Co-current evacuation time was kept low (20 s being the minimum time step considered) since the CO<sub>2</sub> is not retrieved during this step. Other times of the cycle are completely determined by the three times studied as represented by Fig. 2 and the Eqs. (1) and (2). For all the experiments, the time of each step was kept at a minimum of 20 s including the LPP step computed from Eq. (1) and counter-current evacuation step computed from Eq. (2). This limit has been chosen to minimize transient effects in the pilot caused by valve opening, vacuum pump and compressor start-up, etc. Light reflux flow rate bounds were fixed from the characteristics of the vacuum pump, compressor, and flow meter used in the VPSA pilot to maintain a pressure of 0.1 bar at the vacuum pump inlet, and a pressure of 2 bar at the compressor outlet. Co-current evacuation pressure bounds were determined by taking well higher than counter-current evacuation (0.1 bar) but lower than atmospheric pressure since the co-current evacuation is divided in an atmospheric evacuation and vacuum evacuation on the VPSA pilot. Also, the CO<sub>2</sub> remove from the column during this step is released to the atmosphere, which requires to not reduce pressure too low to maintain high recovery.

A response surface methodology was used to study the impact of the five variables on purity and recovery with the results of the design of experiments. This method allows to construct a second order polynomial which can be used to find the optimum operating conditions, and the role of each variable on the results. The polynomial was obtained by fitting the results with the SMT library in python (Saves et al., 2023), and different results were obtained from this polynomial to study the ef-

fect of the five parameters on the purity and recovery. Interaction plots serve as a visual method for evaluating the effect of different variables on the process. In an interaction plot, all variables are set to a mean value defined by the bounds of the variables. Each variable is then changed one by one to assess its impact on the process performance. Additionally, the cross-effect of two variables can be represented by plotting the change of one process metric as function of a variable, while keeping the other variables at different discrete levels. This is represented by a  $k \times k$  grid of plots (where  $k$  is the number of variables studied), with the columns representing one variable continuously changed between its lower and upper bounds, and the rows representing a second variable that changed to different discrete levels (Forrester et al., 2008). The second useful tool is Sobol indices, which allow for a numerical assessment of the variable's impact on the process indicators (Saltelli et al., 2008; Sobol, 2001). Three different indices are generally used: (i) First order, (ii) Second order, and (iii) Total order indices. First order indices provide the direct effect of one variable on the performance of the process, while second order indices reveal the cross-effect of two variables. The sum of first and second order indices should be  $\leq 1$ ; a sum equal to 1 indicates no effect of higher order. Total order indices give an overall view on the effect of each variable on the process indicators. Unlike first and second order indices, the sum of total order indices is  $\geq 1$ . The practical implementation of Sobol indices was carried out using the SALib toolbox available in Python (Iwanaga et al., 2022). This toolbox implements different sensitivity metrics that can be used with any mathematical model, including Sobol indices.

### 2.3. Adsorbent

Two adsorbents were used in the VPSA pilot. Commercial pellets of zeolite 13X (Honeywell Fluka) with a diameter of 1.6 mm were used as reference material. The adsorption columns were slowly filled and shacked to fill the columns of 1.157 L, and to obtain a bulk density of adsorbents as high as possible. The mass of adsorbent was weighed with a scale (+/- 0.1 g of uncertainties) before loading. The same amount of

**Table 2**  
Geometrical parameters of adsorbent used in the VPSA pilot.

	Zeolite 13X	MIL-160(Al)
Mean diameter [mm]	1.61 ± 0.03	2.07 ± 0.06
Mean length [mm]	4.50 ± 0.41	4.20 ± 0.41
Pellet density [kg/m <sup>3</sup> ]	1178.83 ± 17.64	554.65 ± 7.56
Mass per column [g]	800.2 ± 0.2	446 ± 0.2
Bulk density [kg/m <sup>3</sup> ]	691.12 ± 22.19	385.11 ± 12.46
Porosity [m <sup>3</sup> /m <sup>3</sup> ]	0.41 ± 0.03	0.30 ± 0.03

adsorbent was used for the three columns to avoid acyclic phenomena. The adsorbent was regenerated with a heating jacket at 350 °C during 24 h (with a ramp of 1 °C/min and a plateau at 100 °C, and at 180 °C during 2 h) under vacuum (typical lowest pressure of the vacuum pump: 2 Pa). The adsorption columns are then pressurized with nitrogen.

MIL-160(Al) was also tested in the VPSA pilot to evaluate the performance of this MOF for CO<sub>2</sub> capture. The MOF was produced by MOF Technologies, through a thermomechanical route, in a high batch of 60 kg intended for the MOF4AIR industrial pilot. An aliquot of 3 kg from this batch was used for the VPSA pilot of this work. The MIL-160(Al) was shaped in pellets form having a 2 mm diameter. The columns of the VPSA pilot were filled slowly and shacked to have the maximum amount of adsorbent for a volume of 1.157 L. So, according to the sample packing density, the mass of adsorbent is different for the fixed column volume but allows comparison between adsorbents in an adsorption unit (volume fixed). The adsorbent was regenerated under vacuum without heating during 12 h.

The mean size of adsorbent pellets was determined with a caliper (uncertainties of 0.01 mm) by measuring 30 pellets and are given in Table 2, in addition to the mass and the pellet and bulk density calculated. The expressions used for density, porosity and the uncertainty calculations are given in the section 1 of Supporting Information.

Adsorption isotherms of CO<sub>2</sub> and N<sub>2</sub> were measured at three temperatures (20 °C, 30 °C, 40 °C) for both adsorbents by determination of excess adsorbed masses by gravimetric measurement on home-made experimental apparatus described in previous work (Billemont et al., 2017). CO<sub>2</sub> adsorption isotherms were measured from 0 to 1 bar, and N<sub>2</sub> isotherms from 0 to 50 bar for an accurate use of IAST. The experimental data were modelled with a Langmuir model for MIL-160(Al) and N<sub>2</sub> on zeolite 13X, and a dual-site Langmuir model for CO<sub>2</sub> on zeolite 13X (Do, 1998). Working capacity and IAST selectivity were computed from the adsorption isotherms to compare the two materials for the CO<sub>2</sub>/N<sub>2</sub> separation (Bae and Snurr, 2011; Myers and Prausnitz, 1965). The IAST model reasonably predicts the adsorbed quantities for the two systems studied for a 15/85 CO<sub>2</sub>/N<sub>2</sub> mixture (Damasceno Borges et al., 2017; Kim et al., 1994). Adsorption isotherms are presented in Fig. 3 for MIL-160(Al) and Fig. 4 for zeolite 13X. Parameters of the used models are given in the section 3 of the Supporting Information. In addition, four indicators from the literature were used to predict the performance of the adsorbents based on working capacity, selectivity, and heat of adsorption (Table 3). The equations of these metrics are given in the section 3 of Supporting Information.

On mass basis, MIL-160(Al) exhibits a higher working capacity between 0.1 and 2 bar compared to zeolite 13X. This difference is nevertheless compensated by the bulk density of zeolite 13X when the comparison is made on volumetric basis. Selectivity of the zeolite is 20 times higher than MIL-160(Al)'s one which could potentially increase the purities obtained with the zeolite 13X compared to the MOF's one. Regarding the four studied indicators, all values are higher for zeolite 13X except apart the Ackley indicator which is higher for MIL-160(Al) since this indicator only considers the working capacity. Notaro and Yang indicators are at least 10 times higher for zeolite 13X due to the selectivity which is considered for both indicators. Wiersum indicator takes the square root of the selectivity and the squared value of working capacity, and the heat of adsorption which is advantageous for MIL-160(Al). Despite

this, the value of this indicator is still higher for zeolite 13X. It should be noted that the gap between zeolite 13X and MIL-160(Al) is higher if the indicators are computed on volumetric basis, with a higher value of Ackley indicator for zeolite 13X than MIL-160(Al).

### 3. Results and discussion

#### 3.1. Breakthrough curves

Breakthrough curve experiments were performed on the columns of the VPSA pilot described in Section 2.1 which have a height of 30 cm and a diameter of 7.01 cm, without temperature regulation, with both adsorbents described in Section 2.3. The purpose of breakthrough curve measurement is to validate the regeneration of the adsorbent and verify that the three columns have the same behavior for the VPSA cycles. In addition, a breakthrough curve provides an initial comparison of adsorbents via breakthrough times, temperature profile, slope of the curve, ... Breakthrough curves were performed with a flow rate of 1 Nm<sup>3</sup>/h and 15/85%vol. of CO<sub>2</sub>/N<sub>2</sub> mixture. CO<sub>2</sub> concentration at the outlet and temperature inside the column were monitored during the whole experiment. The breakthrough curves are stopped when the concentration of CO<sub>2</sub> at the outlet is equal to 15 %. Adsorbed amount was calculated from the breakthrough curve (Eq. (7) and section 1 of Supporting Information for uncertainties) and was compared to the value obtained through IAST calculation at the same partial pressure and ambient temperature.

$$q = \left( \sum Q_{feed} \cdot (y_{feed} - y_{measured}) \right) / m_{ads} \quad (7)$$

With  $Q_{feed}$  the flow rate of gas,  $y_{feed}$  the CO<sub>2</sub> concentration in the gas,  $y_{measured}$  the CO<sub>2</sub> concentration measured at the outlet of the column, and  $m_{ads}$  the mass of adsorbent.

Breakthrough curves obtained for zeolite 13X in addition to the temperature profile are represented on Fig. 5(a) and (c). The breakthrough time obtained is around 560 s followed by a sharp increase of the CO<sub>2</sub> concentration at the outlet until 10 % CO<sub>2</sub> concentration. The increase of concentration is then slowed with a more flattened curve and a slow increase of CO<sub>2</sub> concentration at the outlet between 12.5 % and 15 %. The change of slope in the breakthrough curve is correlated with the green curve which is the temperature on the 2/3 of the column. The change of slope in breakthrough curve corresponds to the maximum temperature which is 91.6 °C. The slow increase of CO<sub>2</sub> concentrations is due to thermal effect in the column. As the adsorbent is cooling, the CO<sub>2</sub> capacity increases leading to a slow but continuous adsorption of the CO<sub>2</sub>. The maximum CO<sub>2</sub> concentration is obtained when the temperature in the column is stabilized at 28.4 °C. The comparison of the three breakthrough curves performed on zeolite 13X are given in Fig. S2 in Supporting Information. For MIL-160(Al), the breakthrough time is shorter (130 s) due to the lower adsorption capacity and density of the material. The increase of CO<sub>2</sub> concentration follows a sharp increase up to 14 % followed by a slow increase of CO<sub>2</sub> concentration until the maximum value. As for zeolite 13X, this change of slope is correlated with the temperature profile where the maximum temperature (43.7 °C) is reached at the change of slope. Nevertheless, the thermal effects are significantly less important for MIL-160(Al) than for zeolite 13X. The slopes of both breakthrough curves (which are representative of the kinetic of adsorption) are similar and sharp for both adsorbents showing a fast kinetic. The comparison of the three breakthrough curves performed on MIL-160(Al) are given in Fig. S3 in Supporting Information.

The adsorbed amount of CO<sub>2</sub> obtained from the breakthrough curve of zeolite 13X with Eq. (7) is equal to 2.61±0.24 mmol/g. From IAST calculation, the adsorbed amount should be equal to 2.79 mmol/g for a 15/85 % CO<sub>2</sub>/N<sub>2</sub> mixture at 28.4 °C and a pressure of 1.39 bar (which is the pressure measured at the inlet of the column during the experiment). The value of the adsorbed amount is in the confidence interval which seems to indicate an efficient regeneration of the adsorbent and validate the use of IAST for modelling coadsorption isotherms.

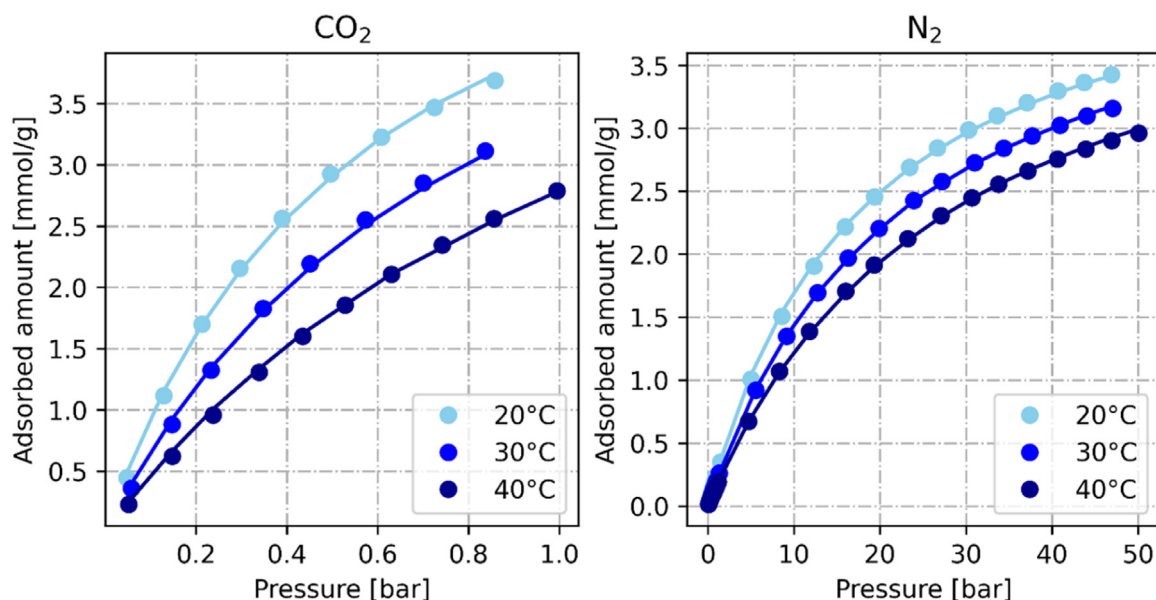


Fig. 3. Adsorption isotherms for CO<sub>2</sub> and N<sub>2</sub> on MIL-160(Al) at 20, 30 and 40 °C. Dots: experimental data, lines: modelling.

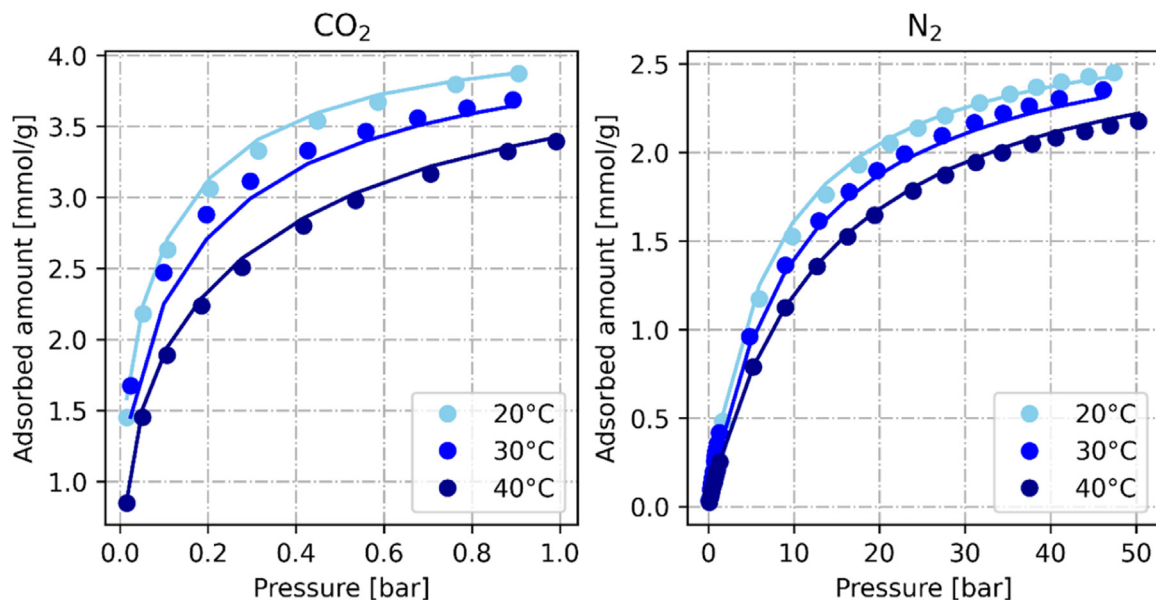


Fig. 4. Adsorption isotherms for CO<sub>2</sub> and N<sub>2</sub> on zeolite 13X at 20, 30 and 40 °C. Dots: experimental data, lines: modelling.

For MIL-160(Al), the adsorbed amount from the breakthrough curve is  $1.41 \pm 0.27$  mmol/g. IAST calculation also gives 1.41 mmol/g for a CO<sub>2</sub>/N<sub>2</sub> mixture of 15.4/84.6 % at 25.1 °C and a pressure of 1.38 bar which validates the sample activation and breakthrough curve measurement.

### 3.2. VPSA cycle

The design of experiments performed on the VPSA pilot and the results obtained for zeolite 13X, and MIL-160(Al) are given in Tables S2 and S3 in the Supporting Information. Recoveries and purities obtained for zeolite 13X and MIL-160(Al) are represented in Fig. 6 with the experimental uncertainties given by the bar determined by the calculation method explained in Section 2 of the Supporting Information. The results obtained demonstrate an overall better performance for the MOF in the studied operating conditions. The best purity obtained for zeolite 13X is equal to 94.5 % with a recovery of 64.5 %. Best recovery

obtained is equal to 85.0 with a purity of 79.7 %. Overall, zeolite 13X fails to meet purity and recovery targets of 95 %. In contrast, for MIL-160(Al), a number of operating conditions give a purity higher than 95 % or recovery higher than 90 %. Nevertheless, both recovery and purity of 95 % cannot be reached. For a purity higher than 95 %, the highest recovery obtained is equal to 88.7 % while for a recovery of at least 95 %, the higher purity is equal to 75.3 %. However, it is possible to reach at least 90 % of recovery and purity with the MIL-160(Al). Table 4 gives the best results obtained for zeolite 13X and MIL-160(Al) and the operating conditions obtained for the experimental points are in the Section 3 of Supporting Information. Despite the results obtained for the four indicators in Table 3, which all showed (except Ackley's indicator on weight basis) that the zeolite 13X was better, MIL-160(Al) performs better for the 3-bed 6-step cycle between 0.1 and 2 bar than zeolite 13X. This clearly illustrates that indicators are not reliable measures of adsorbent's performance while testing the adsorbent in a pilot plant enables their precise evaluation for a given cycle. This step eval-

**Table 3**  
Comparison of indicators for zeolite 13X and MIL-160(Al) for 15/85 CO<sub>2</sub>/N<sub>2</sub> mixture at 20 °C.

	Zeolite 13X	MIL-160(Al)
Mass competitive working capacity between 0.1 and 2 bar [mmol/g]	1.80	1.97
Volumetric competitive working capacity between 0.1 and 2 bar [mmol/cm <sup>3</sup> ]	1.24	0.73
IAST selectivity 0.1 bar [/]	852.53	41.90
IAST selectivity 2 bar [/]	871.04	45.23
CO <sub>2</sub> Heat of adsorption [kJ/mol]	41.21	30.49
Notaro (Notaro et al., 1997) [mmol/g]	1601.91	93.26
Ackley (Ackley et al., 2000) [mmol/g]	6.65	9.77
Yang (Rege and Yang, 2001) [/]	3218.50	231.39
Wiersum (Wiersum et al., 2013) [mmol <sup>3</sup> /(J.g <sup>2</sup> )]	2.32	0.80

**Table 4**  
Best results obtained for zeolite 13X and MIL-160(Al).

	Experiment n°	Purity [%]	Recovery [%]	Energy [kWh/t <sub>CO2</sub> ]	Productivity [t <sub>CO2</sub> /(m <sup>3</sup> <sub>ads</sub> .day)]
Best purity zeolite 13X	3 (13X)	94.5 ± 1.9	64.5 ± 2.1	528.5	1.43 ± 0.05
Best recovery zeolite 13X	23 (13X)	79.7 ± 1.9	85.0 ± 2.8	341.0	1.88 ± 0.06
Purity >95 % MIL-160(Al)	3 (MIL-160)	96.0 ± 1.8	88.7 ± 2.6	312.3	2.00 ± 0.06
Recovery >95 % MIL-160(Al)	36 (MIL-160)	75.3 ± 2.0	95.3 ± 3.4	327.0	2.06 ± 0.07
Recovery and purity >90 % MIL-160(Al)	27 (MIL-160)	90.0 ± 1.8	92.7 ± 2.8	367.7	2.11 ± 0.06

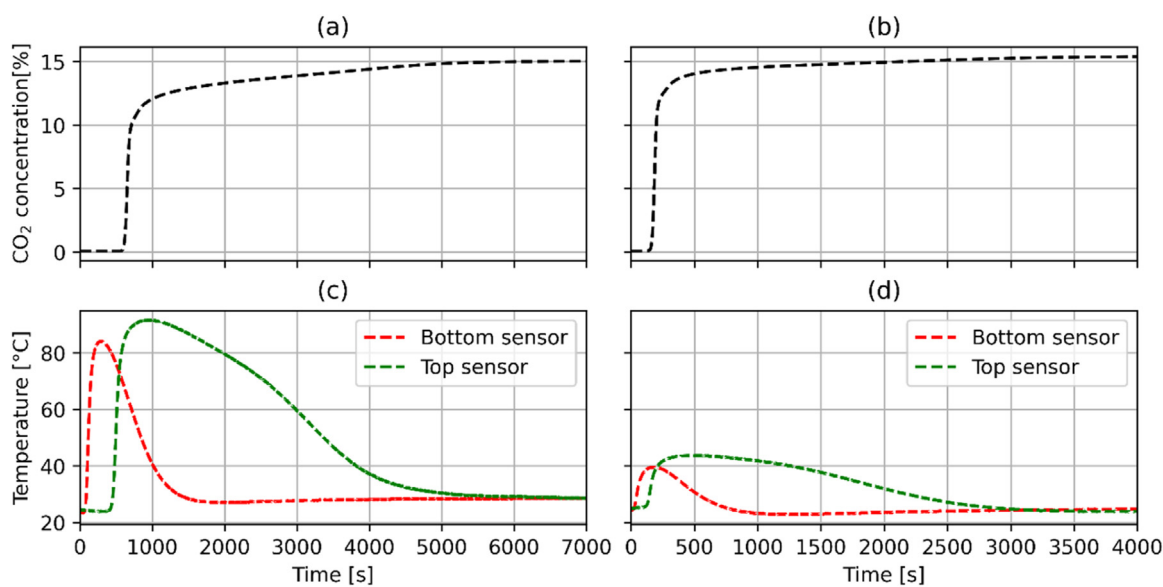


**Fig. 5.** Breakthrough curve and temperature profiles obtained on zeolite 13X and MIL-160(Al). (a): breakthrough curve for zeolite 13X; (b): breakthrough curve for MIL-160(Al); (c): temperature profile for zeolite 13X; (d): temperature profile for MIL-160(Al).

uation at pilot-scale is necessary and crucial in the process of upscaling a material.

Pressure and temperature profiles obtained for the experiment n° 23 with zeolite 13X (best recovery) are represented in Fig. S4 in Supporting Information. Pressure profile is close to the hypothetic profile depicted in Fig. 2 with many perturbations due to the vacuum pump and valve opening/closing during a transition between two steps. For the co-current evacuation, pressure decrease is performed in two stages to avoid sending a higher pressure than atmospheric into the vacuum pump. As observed in temperature profiles, there is an increase of temperature in the bottom of the adsorption column during the adsorption step due to the heat release by zeolite 13X during the adsorption of CO<sub>2</sub>. The increase of temperature in the top of the column is limited probably due to the lower amount of CO<sub>2</sub> in this part. The second temperature increase occurs during the heavy reflux step with a sharp increase

in the bottom of the column and continuous increase in the top part. The increase of CO<sub>2</sub> concentration during this step is responsible of this phenomenon. During the two evacuation steps and the light reflux, the temperature of the whole column decreases due to decrease of pressure, and the desorption of CO<sub>2</sub> to reach around 17.5 °C in the bottom part, and 20 °C in the top part. During light pressure pressurization, the temperature is constant.

The same profiles are given in Fig. S5 in Supporting Information for experiment n°27 of MIL-160(Al) (recovery and purity >90 %). During adsorption step, there is an increase of temperature in the bottom part followed by a plateau, probably due to the saturation of the adsorbent in CO<sub>2</sub>. The top temperature slightly increases during this step. During heavy reflux, we observe a sharp increase for the bottom sensor, reaching temperatures above 30 °C which is higher than zeolite 13X. The increase is less pronounced for the top sensor reaching lower temper-

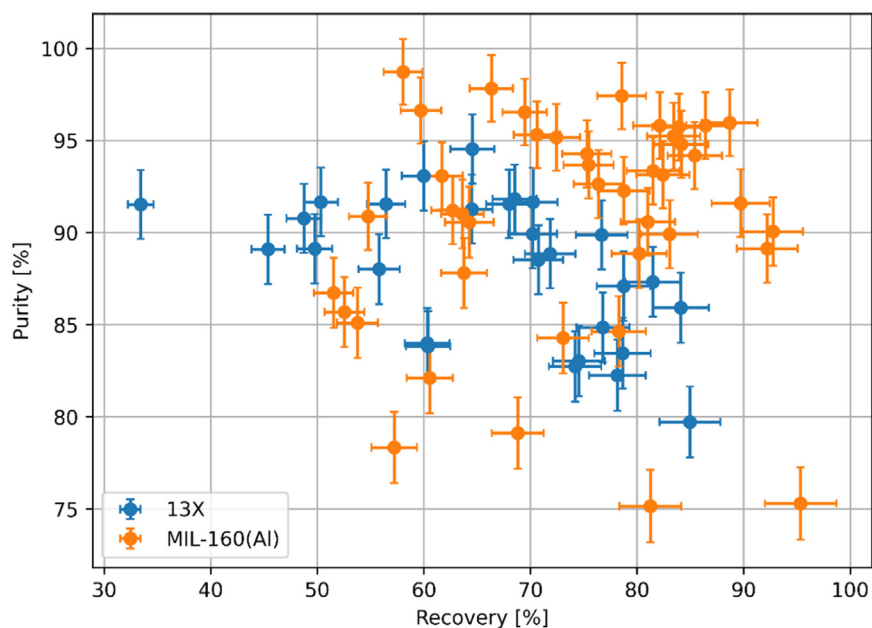


Fig. 6. Recoveries and purities obtained on the VPSA pilot for zeolite 13X and MIL-160(Al).

atures. Evacuations and light reflux lead to a decrease of temperature as for zeolite 13X. The bottom sensor reaches a minimum temperature of 12.8 °C which is well below the minimum of zeolite 13X, indicating a better desorption of the CO<sub>2</sub> for this adsorbent. We can notice a difference of behavior between the both adsorbents during heavy reflux where the MIL-160(Al) seems to adsorb more CO<sub>2</sub> as represented by the higher temperature, and a better desorption of CO<sub>2</sub> for the MOF during light reflux.

Results obtained for zeolite 13X and MIL-160(Al) are similar to the ones listed in Table 1 concerning pilot units from the literature. The range of purity and recovery is similar to those obtained in three pilots operating with zeolite 13X, and the productivity obtained is slightly higher than in the 2-bed pilots. The productivity and energy consumption obtained are similar to those of the pilot of Yu et al. (2022) which is operating for the same flue gas conditions. Nevertheless, the energy consumption is higher, and productivity lower than the simulation made by Khurana & Farooq (2016) on the same VPSA cycle but with different sizes of columns and flow rates giving a gas hourly space velocity four times higher (3300 vs 860 h<sup>-1</sup> for the pilot in this study). Since the sizes of the different pilots found in literature are quite different, an exact comparison between the results of this work and the literature is difficult to make. Pilot of Krishnamurthy et al. (2014) and the pilot of this study have similar GHSV (respectively 928 and 860 h<sup>-1</sup>). In the Krishnamurthy's study, slightly better recoveries (83.4–96.3 %) are obtained but with a lower evacuation pressure (0.025–0.009 bar). Another 3-bed pilot from Zhang et al. (2008) also operates in a similar range of GHSV than this study (873–1521 h<sup>-1</sup>) and reaches the same level of purity with zeolite 13X (90–95 %) but with a slightly lower recovery (60–70 %). The various studies cited above seem to demonstrate that it is possible to achieve high purities, but more difficult to achieve recovery above 90–95 % with zeolite 13X, which is the case with the pilot in this study.

Recoveries and purities were analyzed with the polynomial obtained on the results of the design of experiments. For zeolite 13X, the fitting shows a R<sup>2</sup> of 0.943 for purity and 0.986 for recovery. Actual versus predicted values of the polynomial for zeolite 13X is represented in Fig. S6. Sobol indices (Fig. 7) and interaction plot (Fig. S8) were obtained from the polynomial for zeolite 13X. Total order indices give an overview of the importance of variables while first and second order indices give respectively the direct and combined effects of variables. This study of the impact of the variables allow to identify the important parameters of the process and understand the difference of results between both ad-

sorbents. As represented in Fig. 7, light reflux time is the most important parameter with the highest total and first order indices for both recovery and purity. It should be noted that the time for light reflux and heavy reflux are identical, as these steps take place at the same time, and so this does not indicate that the light reflux step is the most important, but just the time for the step. This is confirmed by the interactions plot where the variable has a strong effect on the results. Nevertheless, the effect of light reflux time is opposite between purity and recovery with an increase of purity and decrease of recovery for high values. This is explained by the heavy reflux step which has the same duration as the light reflux step. Heavy reflux will increase the purity by increasing the amount of CO<sub>2</sub> in the bed, but a part of this CO<sub>2</sub> will be lost during this step. For recovery, the effect of light reflux time is divided between a direct effect and a cross effect with adsorption time ( $t_{ads}$ ,  $t_{LR}$ ) which is more important than direct effect. On the interactions plot, it seems to have an optimum value of light reflux time which is clearly dependent on the adsorption time. For purity, there is also a cross effect between light reflux time and co-current evacuation pressure ( $t_{LR}$ ,  $p_{co-evac}$ ). The effect of this pressure seems to be enhanced for low light reflux time where the best purities are obtained at 0.4 bar. For high light reflux time, the pressure seems to be ineffective on purity. The second most important variable for recovery is adsorption time but it is strongly correlated with the light reflux time as discussed above with almost no first order effect on recovery. Co-current evacuation time and pressure also impact the recovery giving higher value for a pressure of 0.6 bar and a step time of 20 s. The effect of both variables is almost direct with a small interaction between the co-evacuation and light reflux time ( $t_{LR}$ ,  $t_{co-evac}$ ) which is probably representing the counter-current evacuation time. Light reflux flow rate has almost no effect on recovery compared to other variables. For purity, the second most important variable is co-current evacuation pressure with a direct and indirect effect when correlated with light reflux time ( $t_{LR}$ ,  $p_{co-evac}$ ). Best purities are obtained with a pressure of 0.4 bar which is opposite to recovery. Nevertheless, the effect on recovery is more important. Adsorption time also influences purity with an optimum value which is slightly dependent on the other variables. Finally, light reflux flow rate and co-current evacuation time have less effect on purity with an optimal flow rate around 0.2 Nm<sup>3</sup>/h, and an optimum co-current evacuation time depending on other variables.

The same methodology was applied for MIL-160(Al). The polynomial obtained from experimental data gives a R<sup>2</sup> of 0.948 for purity and 0.919 for recovery. The actual versus predicted values is represented on Fig.

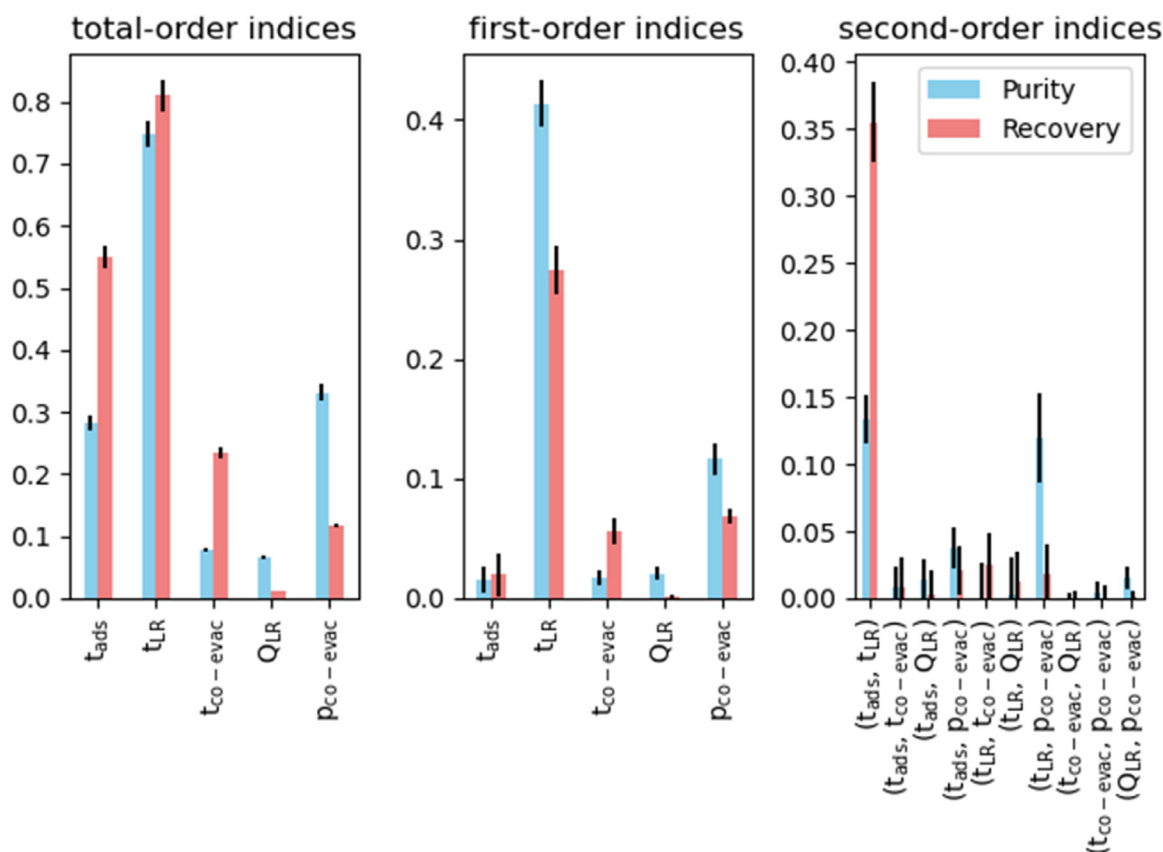


Fig. 7. Sobol indices obtained for zeolite 13X on VPSA pilot.

S7. Interaction plot (Fig. S9), and Sobol indices (Fig. 8) were obtained from the polynomial as for zeolite 13X. Light reflux time is also the main parameter for purity obtained on MIL-160(Al) with an important first order effect. As represented on interaction plot, an increase of light reflux time leads to an important increase of purity. There is also a weak interaction with adsorption time as represented by the second-order indices ( $t_{ads}$ ,  $t_{LR}$ ). The other variables have a low influence on purity as represented by the total order indices obtained for MIL-160(Al). The adsorption time has a weak direct effect and an indirect effect with light reflux time which is described above. On interactions plot, adsorption time has a U-shape with a minimum purity which depends on other variables. Co-current evacuation pressure slightly changes the purity directly. The better purities were obtained for a pressure of 0.4 bar. Light reflux flow rate and co-current evacuation time have almost no effect on purity with flat blue curves on the interactions plot. Recovery is driven equally by adsorption and light reflux times. There is a direct effect for both variables and second-order effect between adsorption and light reflux time ( $t_{ads}$ ,  $t_{LR}$ ) which is more important than the direct effect of the variables which could represent the counter-current evacuation time. The effect of adsorption time on recovery is totally changed by the light reflux time as represented on the interaction plot. In a similar way, the optimum value of light reflux time is shifted with the adsorption time. Adsorption time has also interaction effect with light reflux flow rate ( $t_{ads}$ ,  $Q_{LR}$ ), and the light reflux time has interaction effect with the light reflux flow rate ( $t_{LR}$ ,  $Q_{LR}$ ) and the co-current evacuation time ( $t_{LR}$ ,  $t_{co-evac}$ ). The third most important variable is the light reflux flow rate with an optimum value for recovery around 0.2  $Nm^3/h$  which can be slightly shifted by light reflux time ( $t_{LR}$ ,  $Q_{LR}$ ) and co-current evacuation time ( $Q_{LR}$ ,  $t_{co-evac}$ ) and pressure ( $Q_{LR}$ ,  $p_{co-evac}$ ). Co-current evacuation time has a direct impact on recovery with lower time leading to higher recoveries. There is a weak interaction effect with light reflux time ( $t_{LR}$ ,  $t_{co-evac}$ ). Finally, the co-current evacuation pres-

sure has the weakest impact on recovery with best recoveries obtained at 0.6 bar.

The main difference between zeolite 13X and MIL-160(Al) is the impact of the light reflux step on the results. For zeolite 13X, an increase of light reflux time will lead to a sharp decrease of recovery with a low increase of purity as if the  $CO_2$  sent during the heavy reflux step was largely lost. On the other hand, the increase of light reflux time for MIL-160(Al) will lead to an increase of purity. Recovery will increase until a maximum value is reached before decreasing. The difference of results and behaviors could be explained by the difference of  $CO_2$  and  $N_2$  adsorption isotherms. During the heavy reflux step, the  $CO_2$  concentration sent to the adsorption bed is higher than 50 % giving a partial pressure of  $CO_2$  higher than 1 bar while adsorption pressure is 2 bar. The shape of the  $CO_2$  adsorption isotherms of zeolite 13X is very steep at low partial pressures but exhibits a plateau shape for partial pressures higher than 0.5 bar. For MIL-160(Al), the slope of the  $CO_2$  adsorption isotherms is more or less constant between 0 and 1 bar. This difference of slopes can explain the different behaviors during the heavy reflux step: zeolite 13X is almost saturated before this step which can explain the decrease of recovery. The low change in adsorbed amount can also explain the low change in purity obtained. In contrast, the adsorbed amount of MIL-160(Al) will sharply increase during the heavy reflux step, leading to higher purity. The maximum of recovery when increasing the light reflux time can be interpreted as the limit before the saturation of the bed. Nitrogen adsorption isotherms also play an important role in VPSA processes. Rajagopalan & Rajendran (2018) have demonstrated that low nitrogen affinity ( $b$  in the Langmuir model) is more important than selectivity when the  $CO_2/N_2$  selectivity is higher than 11.4. In this case, the nitrogen affinity for zeolite 13X is almost two times higher than the nitrogen affinity of MIL-160(Al) at 20 °C (0.135 1/bar vs 0.057 1/bar). This difference probably allows the reduction of the adsorbed nitrogen amount which leads to higher purity and to perform the light reflux

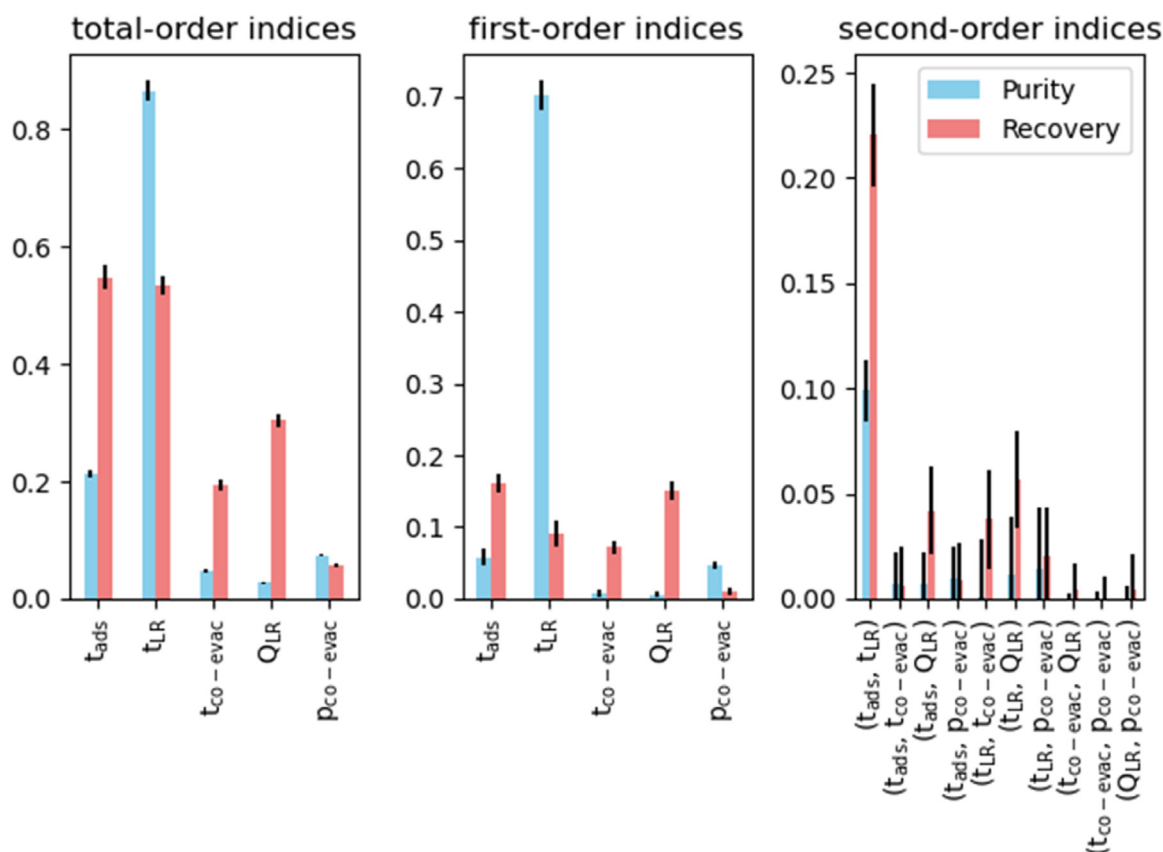


Fig. 8. Sobol indices obtained for MIL-160(Al) on VPSA pilot.

step adsorbing very little nitrogen. For the co-current evacuation step, the low adsorbed amount of nitrogen will lead to higher purity during counter-current evacuation.

#### 4. Conclusion

In this work, a VPSA pilot unit, made up of 3 beds of 1.157 L, was developed and built to perform breakthrough curves, 2-bed and 3-bed VPSA cycles. Zeolite 13X was selected as benchmark material while the microporous bioderived Al-MOF, MIL-160(Al), was synthesized and shaped at 60 kg scale as promising alternative for CO<sub>2</sub> capture from flue gases. They were both tested in this installation to evaluate their performance for the separation of a 15/85 % CO<sub>2</sub>/N<sub>2</sub> mixture with a 3-bed 6-step cycle for post-combustion CO<sub>2</sub> capture process. Best results were obtained with MIL-160(Al) which can reach 90 % of purity and recovery at the same time or 95 % purity and 95 % recovery independently. This proves the performance of this selected MOF, which is capable of competing with traditional adsorbents for CO<sub>2</sub> capture. MIL-160(Al) is also easier to activate (no heating required) and remained stable throughout the tests. Results obtained in terms of purity and recovery differ from those obtained using classical indicators, which predict better performance for zeolite 13X. The evaluation of an adsorbent on a kilogram scale is undeniably an important step in the development of a new material. Testing in a VPSA pilot unit allows to verify the adsorbent's behavior in terms of regeneration and cycle operation. In addition, the pilot-scale test provides the material's performance in terms of purity and recovery, two indicators used on an industrial scale for a CO<sub>2</sub> capture process. The impact of the different variables of the VPSA pilot were studied for both adsorbents giving the impact of the parameters on recovery and purity. Light reflux step is the main difference between zeolite 13X and MIL-160(Al) showing different behaviors depending on the material. It could be explained by the shape of adsorption isotherms

of the materials which are not similar. These results enabled the identification of the most important parameters of the cycle studied. This could reduce the number of variables to be studied for future industrial-scale tests. The flexible pilot developed in this work could be used with other new adsorbents to evaluate their performance in a similar way to what has been done in this work. In addition, other cycles could be carried out to study cycle performance and the various parameters involved. Results obtained with the laboratory scale pilot will be used and compared with the industrial pilot of the MOF4AIR project results using the same MOF and showing how the scaling up of the process influences the performance.

#### Declaration of competing interest

The authors declare that they have no known competing financial interests or personal relationships that could have appeared to influence the work reported in this paper.

#### CRediT authorship contribution statement

**A. Henrotin:** Writing – review & editing, Writing – original draft, Visualization, Validation, Methodology, Investigation, Formal analysis, Data curation, Conceptualization. **N. Heymans:** Writing – review & editing, Writing – original draft, Validation, Supervision, Methodology, Investigation, Data curation, Conceptualization. **M.E. Duprez:** Writing – review & editing, Project administration. **G. Mouchaham:** Writing – review & editing, Resources, Conceptualization. **C. Serre:** Writing – review & editing, Resources, Funding acquisition, Conceptualization. **D. Wong:** Resources. **R. Robinson:** Resources. **D. Mulrooney:** Resources. **J. Casaban:** Writing – review & editing, Resources, Funding acquisition. **G. De Weireld:** Writing – review & editing, Validation, Supervision, Project administration, Funding acquisition, Conceptualization.

## Acknowledgments

This project has received funding from the European Union's Horizon 2020 research and innovation program under grant agreement No. 831975. This output reflects only the author's view and the European Union cannot be held responsible for any use that may be made of the information contained therein.

## Supplementary materials

Supplementary material associated with this article can be found, in the online version, at [doi:10.1016/j.ccs.2024.100224](https://doi.org/10.1016/j.ccs.2024.100224).

## References

- Ackley, M.W., Stewart, A.B., Henzler, G.W., Leavitt, F.W., Notaro, F., & Kane, M.S. (2000). PSA apparatus and process using adsorbent mixtures. In *Patent and Trademark Office*.  
 Ahn, H., Luberti, M., Liu, Z., Brandani, S., 2013. Process configuration studies of the amine capture process for coal-fired power plants. *Int. J. Greenh. Gas Control* 16, 29–40. doi:10.1016/j.ijggc.2013.03.002.  
 Andersen, A., Divekar, S., Dasgupta, S., Cavka, J.H., Aarti, A., Nanoti, A., Spjelkavik, A., Goswami, A.N., Garg, M.O., Blom, R., 2013. On the development of Vacuum Swing Adsorption (VSA) technology for post-combustion CO<sub>2</sub> capture. *Energy Procedia* 37 (1876), 33–39. doi:10.1016/j.egypro.2013.05.082.  
 Bae, Y.S., Snurr, R.Q., 2011. Development and evaluation of porous materials for carbon dioxide separation and capture. *Angewan. Chem. Int. Edit.* 50 (49), 11586–11596. doi:10.1002/anie.201101891.  
 Bhattacharyya, D., Miller, D.C., 2017. Post-combustion CO<sub>2</sub> capture technologies — a review of processes for solvent-based and sorbent-based CO<sub>2</sub> capture. *Curr. Opin. Chem. Eng.* 17, 78–92. doi:10.1016/j.coche.2017.06.005.  
 Billemont, P., Heymans, N., Normand, P., De Weireld, G., 2017. IAST predictions vs co-adsorption measurements for CO<sub>2</sub> capture and separation on MIL-100 (Fe). *Adsorption* 23 (2–3), 225–237. doi:10.1007/s10450-016-9825-6.  
 Brandt, P., Nuhn, A., Lange, M., Möllmer, J., Weingart, O., Janiak, C., 2019. Metal-organic frameworks with potential application for SO<sub>2</sub> separation and flue gas desulfurization. *ACS Appl. Mater. Interfaces* 11 (19), 17350–17358. doi:10.1021/ac-sami.9b00029.  
 Cadiau, A., Lee, J.S., Damasceno Borges, D., Fabry, P., Devic, T., Wharmby, M.T., Martineau, C., Foucher, D., Taulelle, F., Jun, C.H., Hwang, Y.K., Stock, N., De Lange, M.F., Kapteijn, F., Gascon, J., Maurin, G., Chang, J.S., Serre, C., 2015. Design of hydrophilic metal organic framework water adsorbents for heat reallocation. *Adv. Mater.* 27 (32), 4775–4780. doi:10.1002/adma.201502418.  
 Chue, K.T., Kim, J.N., Yoo, Y.J., Cho, S.H., Yang, R.T., 1995. Comparison of activated carbon and zeolite 13X for CO<sub>2</sub> recovery from flue gas by pressure swing adsorption. *Ind. Eng. Chem. Res.* 34 (2), 591–598. doi:10.1021/ie00041a020.  
 Damasceno Borges, D., Normand, P., Permiakova, A., Babarao, R., Heymans, N., Galvao, D.S., Serre, C., De Weireld, G., Maurin, G., 2017. Gas adsorption and separation by the Al-based metal-organic framework MIL-160. *J. Phys. Chem. C* 121 (48), 26822–26832. doi:10.1021/acs.jpcc.7b08856.  
 Dasgupta, S., Biswas, N., Aarti, Gode, N. G., Divekar, S., Nanoti, A., Goswami, A.N., 2012. CO<sub>2</sub> recovery from mixtures with nitrogen in a vacuum swing adsorbent using metal organic framework adsorbent: a comparative study. *Int. J. Greenh. Gas Control* 7, 225–229. doi:10.1016/j.ijggc.2011.10.007.  
 Do, D.D. (1998). *Fundamentals of diffusion and adsorption in porous media* (Vol. 2). 10.1142/9781860943829\_0007.  
 Edubilli, S., Gumma, S., 2019. A systematic evaluation of UiO-66 metal organic framework for CO<sub>2</sub>/N<sub>2</sub> separation. *Sep. Purif. Technol.* 224, 85–94. doi:10.1016/j.seppur.2019.04.081, (April).  
 Forrester, A. I. J., Söbester, A., Keane, A. J., 2008. *Engineering Design via Surrogate Modelling*. Wiley. <https://doi.org/10.1002/9780470770801>.  
 Glier, J.C., Rubina, E.S., 2013. Assessment of solid sorbents as a competitive post-combustion CO<sub>2</sub> capture technology. *Energy Procedia* 37, 65–72. doi:10.1016/j.egypro.2013.05.086.  
 Grande, C.A., 2012. Advances in pressure swing adsorption for gas separation. *ISRN Chem. Eng.* 2012, 1–13. doi:10.5402/2012/982934.  
 Haghpanah, R., Majumder, A., Nilam, R., Rajendran, A., Farooq, S., Karimi, I.A., Amanullah, M., 2013a. Multiobjective optimization of a four-step adsorption process for postcombustion CO<sub>2</sub> capture via finite volume simulation. *Ind. Eng. Chem. Res.* 52 (11), 4249–4265. doi:10.1021/ie302658y.  
 Haghpanah, R., Nilam, R., Rajendran, A., Farooq, S., Karimi, I.A., 2013b. Cycle synthesis and optimization of a VSA process for postcombustion CO<sub>2</sub> capture. *AIChE J.* 59 (12), 4735–4748. doi:10.1002/aic.14192.  
 Heymans, N., Duprez, M.E., De Weireld, G., 2021. MOF4AIR Project (H2020): metal organic frameworks for carbon dioxide adsorption processes in power production and energy intensive industries. *SSRN Electr. J.* doi:10.2139/ssrn.3821559, March.  
 Hong, W.Y., 2022. A techno-economic review on carbon capture, utilisation and storage systems for achieving a net-zero CO<sub>2</sub> emissions future. *Carbon Capture Sci. Technol.* 3, 100044. doi:10.1016/j.ccs.2022.100044, (March).  
 Hu, Z., Wang, Y., Shah, B.B., Zhao, D., 2019. CO<sub>2</sub> capture in metal-organic framework adsorbents: an engineering perspective. *Adv. Sustain. Syst.* 3 (1), 1800080. doi:10.1002/adsu.201800080.  
 IEA, 2023. CO<sub>2</sub> emissions in 2022. CO<sub>2</sub> Emissions in 2022. OECD doi:10.1787/12ad1e1a-en.  
 IEA (2020). (2020). Energy technology perspectives 2020 - special report on carbon capture utilisation and storage. IEA. 10.1787/208b66f4-en.  
 IPCC. (2021). Assessment report 6 climate change 2021: the physical science basis. In *Climate change 2021: the physical science basis. contribution of working group I to the sixth assessment report of the intergovernmental panel on climate change*. <https://www.ipcc.ch/report/ar6/wgl1/>.  
 Iwanaga, T., Usher, W., Herman, J., 2022. Toward SALib 2.0: Advancing the accessibility and interpretability of global sensitivity analyses. *Socio-Environmental Systems Modelling* 4, 18155. <https://doi.org/10.18174/sesmo.18155>.  
 Kárászová, M., Zach, B., Petrusová, Z., Červenka, V., Bobák, M., Šyc, M., Izák, P., 2020. Post-combustion carbon capture by membrane separation. *Rev. Sep. Purif. Technol.* 238. doi:10.1016/j.seppur.2019.116448, (December 2019).  
 Karimi, M., Ferreira, A., Rodrigues, A.E., Nouar, F., Serre, C., Silva, J.A.C., 2023. MIL-160(Al) as a candidate for biogas upgrading and CO<sub>2</sub> capture by adsorption processes. *Ind. Eng. Chem. Res.* 62 (12), 5216–5229. doi:10.1021/acs.iecr.2c04150.  
 Khoo, H.H., Tan, R.B.H., 2006. Life cycle investigation of CO<sub>2</sub> recovery and sequestration. *Environ. Sci. Technol.* 40 (12), 4016–4024. doi:10.1021/es051882a.  
 Khurana, M., Farooq, S., 2016. Simulation and optimization of a 6-step dual-reflux VSA cycle for post-combustion CO<sub>2</sub> capture. *Chem. Eng. Sci.* 152, 507–515. doi:10.1016/j.ces.2016.06.033.  
 Kim, J.N., Chue, K.T., Kim, K.I.L., Cho, S.H., Kim, J.D., 1994. Non-isothermal adsorption of nitrogen-carbon dioxide mixture in a fixed bed of zeolite-X. *J. Chem. Eng. Jpn.* 27 (1), 45–51. doi:10.1252/jcej.27.45.  
 Krishnamurthy, S., Rao, V.R., Guntuka, S., Sharratt, P., Haghpanah, R., Rajendran, A., Amanullah, M., Karimi, I.A., Farooq, S., 2014. CO<sub>2</sub> capture from dry flue gas by vacuum swing adsorption: a pilot plant study. *AIChE J.* 60 (5), 1830–1842. doi:10.1002/aic.14435.  
 Lamb, W. F., Wiedmann, T., Pongratz, J., Andrew, R., Crippa, M., Olivier, J. G. J., Wiedenhofer, D., Mattioli, G., Khourdaji, A. Al, House, J., Pachauri, S., Figueroa, M., Saheb, Y., Slade, R., Hubacek, K., Sun, L., Ribeiro, S. K., Khennas, S., de la Rue du Can, S., Chapungu, L., Davis, S.J., Bashmakov, I., Dai, H., Dhakal, S., Tan, X., Geng, Y., Gu, B., Minx, J. (2021). A review of trends and drivers of greenhouse gas emissions by sector from 1990 to 2018. *Environmental Research Letters*, 16(7), 073005. <https://doi.org/10.1088/1748-9326/abee4e>.  
 Lin, J.Bin, Nguyen, T.T.T., Vaidhyanathan, R., Burner, J., Taylor, J.M., Durekova, H., Akhtar, F., Mah, R.K., Ghaffari-Nik, O., Marx, S., Fylstra, N., Iremonger, S.S., Dawson, K.W., Sarkar, P., Hovington, P., Rajendran, A., Woo, T.K., Shimizu, G.K.H., 2021. A scalable metal-organic framework as a durable physisorbent for carbon dioxide capture. *Science* (1979) 374 (6574), 1464–1469. doi:10.1126/science.abi7281.  
 Liu, Z., Wang, L., Kong, X., Li, P., Yu, J., Rodrigues, A.E., 2012. Onsite CO<sub>2</sub> capture from flue gas by an adsorption process in a coal-fired power plant. *Ind. Eng. Chem. Res.* 51 (21), 7355–7363. doi:10.1021/ie3005308.  
 Lyu, P., Maurin, G., 2021. H<sub>2</sub>S stability of metal-organic frameworks: a computational assessment. *ACS Appl. Mater. Interfaces* 13 (3), 4813–4822. doi:10.1021/ac-sami.0c21285.  
 Majchrzak-Kucęba, I., Wawrzyńczak, D., Ściubido, A., 2019. Application of metal-organic frameworks in VPSA technology for CO<sub>2</sub> capture. *Fuel* 255. doi:10.1016/j.fuel.2019.115773, (October 2018).  
 Masala, A., Vitillo, J.G., Mondino, G., Grande, C.A., Blom, R., Manzoli, M., Marshall, M., Bordiga, S., 2017. CO<sub>2</sub> capture in dry and wet conditions in UTSA-16 metal-organic framework. *ACS Appl. Mater. Interfaces* 9 (1), 455–463. doi:10.1021/ac-sami.6b13216.  
 Mondal, M.K., Balsora, H.K., Varshney, P., 2012. Progress and trends in CO<sub>2</sub> capture/separation technologies: a review. *Energy* 46 (1), 431–441. doi:10.1016/j.energy.2012.08.006.  
 Myers, A.L., Prausnitz, J.M., 1965. Thermodynamics of mixed-gas adsorption. *AIChE J.* 11 (1), 121–127.  
 NETL. (2023). *Point source carbon capture program. August*. <https://www.netl.doe.gov/carbon-management/carbon-capture>.  
 Nguyen, T.T.T., Lin, J.Bin, Shimizu, G.K.H., Rajendran, A., 2022. Separation of CO<sub>2</sub> and N<sub>2</sub> on a hydrophobic metal organic framework CALF-20. *Chem. Eng. J.* 442 (P2), 136263. doi:10.1016/j.cej.2022.136263.  
 Nguyen, T.T.T., Shimizu, G.K.H., Rajendran, A., 2023. CO<sub>2</sub>/N<sub>2</sub> separation by vacuum swing adsorption using a metal-organic framework, CALF-20: multi-objective optimization and experimental validation. *Chem. Eng. J.* 452 (P4), 139550. doi:10.1016/j.cej.2022.139550.  
 Notaro, F., Mullhaupt, J.T., Wells, F.W., & Ackley, M.W. (1997). *Adsorption process and system using multilayer adsorbent beds*. <https://patents.google.com/patent/US5810909>.  
 Permyakova, A., Skrylnyuk, O., Courbon, E., Affram, M., Wang, S., Lee, U.H., Valekar, A.H., Nouar, F., Mouchaham, G., Devic, T., De Weireld, G., Chang, J.S., Steunou, N., Frère, M., Serre, C., 2017. Synthesis optimization, shaping, and heat reallocation evaluation of the hydrophilic metal-organic framework MIL-160(Al). *ChemSusChem* 10 (7), 1419–1426. doi:10.1002/cssc.201700164.  
 Raganati, F., Miccio, F., Ammendola, P., 2021. Adsorption of carbon dioxide for post-combustion capture: a review. *Energy Fuels* 35 (16), 12845–12868. doi:10.1021/acs.energyfuels.1c01618.  
 Rajagopalan, A.K., Avila, A.M., Rajendran, A., 2016. Do adsorbent screening metrics predict process performance? A process optimisation based study for post-combustion capture of CO<sub>2</sub>. *Int. J. Greenh. Gas Control* 46, 76–85. doi:10.1016/j.ijggc.2015.12.033.  
 Rajagopalan, A.K., Rajendran, A., 2018. The effect of nitrogen adsorption on vacuum swing adsorption based post-combustion CO<sub>2</sub> capture. *Int. J. Greenh. Gas Control* 78, 437–447. doi:10.1016/j.ijggc.2018.09.002, July.

- Rege, S.U., Yang, R.T., 2001. A simple parameter for selecting an adsorbent for gas separation by pressure swing adsorption. *Sep. Sci. Technol.* 36 (15), 3355–3365. doi:10.1081/SS-100107907.
- Riboldi, L., Bolland, O., 2017. Overview on Pressure Swing Adsorption (PSA) as CO<sub>2</sub> capture technology: state-of-the-art, limits and potentials. *Energy Procedia* 114 (1876), 2390–2400. doi:10.1016/j.egypro.2017.03.1385.
- Rogelj, J., Den Elzen, M., Höhne, N., Fransen, T., Fekete, H., Winkler, H., Schaeffer, R., Sha, F., Riahi, K., Meinshausen, M., 2016. Paris agreement climate proposals need a boost to keep warming well below 2 °C. *Nature* 534 (7609), 631–639. doi:10.1038/nature18307.
- Ruthven, D., 1984. *Principles of Adsorption and Adsorption Processes (First)*. John Wiley & Sons.
- Saltelli, A., Ratto, M., Andres, T., Campolongo, F., Cariboni, J., Gatelli, D., Saisana, M., Tarantola, S., 2008. Global Sensitivity Analysis: The Primer. <https://doi.org/10.1002/9780470725184>.
- Saves, P., Lafage, R., Bartoli, N., Diouane, Y., Bussemaker, J., Lefebvre, T., Hwang, J. T., Morlier, J., Martins, J. R. R. A., 2020. SMT 2.0: A Surrogate Modeling Toolbox with a focus on Hierarchical and Mixed Variables Gaussian Processes.
- Shen, C., Yu, J., Li, P., Grande, C.A., Rodrigues, A.E., 2011. Capture of CO<sub>2</sub> from flue gas by vacuum pressure swing adsorption using activated carbon beads. *Adsorption* 17 (1), 179–188. doi:10.1007/s10450-010-9298-y.
- Sifat, N.S., Haseli, Y., 2019. A critical review of CO<sub>2</sub> capture technologies and prospects for clean power generation. *Energies (Basel)* 12 (21). doi:10.3390/en12214143.
- Simoni, M., Wilkes, M.D., Brown, S., Provis, J.L., Kinoshita, H., Hanein, T., 2022. Decarbonising the lime industry: state-of-the-art. *Renew. Sustain. Energy Rev.* 168, 112765. doi:10.1016/j.rser.2022.112765, (April).
- Skarstrom, C.W. (1960). *Method and apparatus for fractionating gaseous mixtures by adsorption* (Patent No. US2944627).
- Sobol, I. M., 2001. Global sensitivity indices for nonlinear mathematical models and their Monte Carlo estimates. *Mathematics and Computers in Simulation* 55 (1–3), 271–280. [https://doi.org/10.1016/S0378-4754\(00\)00270-6](https://doi.org/10.1016/S0378-4754(00)00270-6).
- Song, C., Liu, Q., Deng, S., Li, H., Kitamura, Y., 2019. Cryogenic-based CO<sub>2</sub> capture technologies: state-of-the-art developments and current challenges. *Renew. Sustain. Energy Rev.* 101, 265–278. doi:10.1016/j.rser.2018.11.018, (July 2018).
- Sumida, K., Rogow, D.L., Mason, J.A., Mcdonald, T.M., Bloch, E.D., Herm, Z.R., Bae, T., Long, R., 2012. Carbon dioxide capture in meta-organic frameworks. *Chem. Rev.* 112, 724–781.
- UNFCCC. (2022). Glasgow Cop26 on climate change conference. *Decisions adopted by the conference of the parties serving as the meeting of the parties to the Paris Agreement, March*, 1–46. [https://unfccc.int/sites/default/files/resource/cma2021\\_10E.pdf](https://unfccc.int/sites/default/files/resource/cma2021_10E.pdf).
- Vega, F., Baena-Moreno, F.M., Gallego Fernández, L.M., Portillo, E., Navarrete, B., Zhang, Z., 2020. Current status of CO<sub>2</sub> chemical absorption research applied to CCS: towards full deployment at industrial scale. *Appl. Energy* 260, 114313. doi:10.1016/j.apenergy.2019.114313, (October 2019).
- Wahiduzzaman, M., Lenzen, D., Maurin, G., Stock, N., Wharmby, M.T., 2018. Rietveld refinement of MIL-160 and its structural flexibility upon H<sub>2</sub>O and N<sub>2</sub> adsorption. *Eur. J. Inorg. Chem.* (32) 3626–3632. doi:10.1002/ejic.201800323, 2018.
- Wang, L., Liu, Z., Li, P., Wang, J., Yu, J., 2012. CO<sub>2</sub> capture from flue gas by two successive VPSA units using 13XAPG. *Adsorption* 18 (5–6), 445–459. doi:10.1007/s10450-012-9431-1.
- Wang, L., Yang, Y., Shen, W., Kong, X., Li, P., Yu, J., Rodrigues, A.E., 2013. Experimental evaluation of adsorption technology for CO<sub>2</sub> capture from flue gas in an existing coal-fired power plant. *Chem. Eng. Sci.* 101, 615–619. doi:10.1016/j.ces.2013.07.028.
- Webley, P.A., Qader, A., Ntiamoah, A., Ling, J., Xiao, P., Zhai, Y., 2017. A new multi-bed vacuum swing adsorption cycle for CO<sub>2</sub> capture from flue gas streams. *Energy Procedia* 114, 2467–2480. doi:10.1016/j.egypro.2017.03.1398, (November 2016).
- Wiersum, A.D., Chang, J.S., Serre, C., Llewellyn, P.L., 2013. An adsorbent performance indicator as a first step evaluation of novel sorbents for gas separations: application to metal-organic frameworks. *Langmuir*. 29 (10), 3301–3309. doi:10.1021/la3044329.
- Younas, M., Rezakazemi, M., Daud, M., Wazir, M.B., Ahmad, S., Ullah, N., Inamuddin, Ramakrishna, S., 2020. Recent progress and remaining challenges in post-combustion CO<sub>2</sub> capture using metal-organic frameworks (MOFs). *Prog. Energy Combust. Sci.* 80. doi:10.1016/j.peccs.2020.100849.
- Yu, J., Balbuena, P.B., 2013. Water effects on postcombustion CO<sub>2</sub> capture in Mg-MOF-74. *J. Phys. Chem. C* 117 (7), 3383–3388. doi:10.1021/jp311118x.
- Yu, X., Liu, B., Shen, Y., Zhang, D., 2022. Design and experiment of high-productivity two-stage vacuum pressure swing adsorption process for carbon capturing from dry flue gas. *Chin. J. Chem. Eng.* 43, 378–391. doi:10.1016/j.cjche.2021.02.022.
- Zhang, J., Webley, P.A., Xiao, P., 2008. Effect of process parameters on power requirements of vacuum swing adsorption technology for CO<sub>2</sub> capture from flue gas. *Energy Convers. Manage* 49 (2), 346–356. doi:10.1016/j.enconman.2007.06.007.
- Zhao, R., Deng, S., Zhao, L., Zhao, Y., Li, S., Zhang, Y., Yu, Z., 2017. Experimental study and energy-efficiency evaluation of a 4-step pressure-vacuum swing adsorption (PVSA) for CO<sub>2</sub> capture. *Energy Convers. Manage* 151, 179–189. doi:10.1016/j.enconman.2017.08.057, (August).